Assessment of landslide susceptibility for Meghalaya in North Eastern Region of India using bivariate and multi-criteria decision analysis models

Navdeep Agrawal
Shiv Nadar University
Jagabandhu Dixit (jagabandhu.dixit@snu.edu.in)
Shiv Nadar University https://orcid.org/0000-0002-5450-578X

Research Article

Keywords: Landslide, GIS, AHP, Fuzzy, Entropy, Northeast India, Hazard, AUC

Posted Date: October 21st, 2021

DOI: https://doi.org/10.21203/rs.3.rs-993819/v1

Version of Record: A version of this preprint was published at All Earth on April 27th, 2022. See the published version at https://doi.org/10.1080/27669645.2022.2101256.

Assessment of landslide susceptibility for Meghalaya in North Eastern Region of India using bivariate and multi-criteria decision analysis models

Navdeep Agrawal, Jagabandhu Dixit*

Disaster Management Laboratory, Shiv Nadar University, Delhi NCR, Greater Noida, Uttar Pradesh 201314, India

E-mail address of authors: na655@snu.edu.in; jagabandhu.dixit@snu.edu.in

***Corresponding Author:** Jagabandhu Dixit, Email: jagabandhu.dixit@snu.edu.in

Abstract

The state of Meghalaya of the North Eastern Region (NER) of India, situated in the India Himalayan Region (IHR), is the rainiest place in the country and falls under seismic zone V. The Himalayan ranges account for 80% of total landslide hazards in India. The main goal of the present study is to generate the GIS-based landslide susceptibility map (LSM) of Meghalaya by using frequency ratio (FR), Shannon entropy (SE), analytical hierarchy process (AHP), and fuzzy-AHP (FAHP) models and compare these models for the study area. Fifteen landslide conditioning factors are used for susceptibility mapping includes a slope, aspect, elevation, plan curvature, stream power index (SPI), topographic wetness index (TWI), land use land cover (LULC), normalized difference vegetation index (NDVI), distance from the river, road and faults, rainfall (30 years mean annual rainfall), soil texture, geomorphology, and lithology. Landslide inventory of 1330 landslide events is prepared and mapped from various sources. The inventory dataset is randomly split in a 70/30 ratio to make the training dataset (70%) used in the model and testing dataset (remaining 30%) for validation purposes. The southern escarpment, the southeast region of the study area, and hillslope along the roadside show high susceptibility for landslide occurrence in all four models. The LSMs produced in the present study are validated using the area under curve (AUC) value. The

presented LSMs can help concerned authorities and planners to make sustainable development plans and formulate risk mitigation strategies keeping in mind the critical areas for landslide hazards.

Keywords: Landslide, GIS, AHP, Fuzzy, Entropy, Northeast India, Hazard, AUC

1. Introduction

Landslide is a natural disaster, defined as the movement of a mass of rock, debris, or soil mass down a slope. It is one of the most frequently occurring natural hazards and has caused massive damage to infrastructure, human settlements, and loss of lives worldwide. After China, India is the second most affected country in Asia by this disaster, as per the Centre for Research on the Epidemiology of Disasters (CRED) (Guha-Sapir et al. 2012). The entire Himalayan range of India is very susceptible to landslides which accounts for approximately 80% of total landslide events in the country (Onagh et al. 2012). Due to landslides, significant damage to roads and other infrastructure, economic and human losses have been reported in Himalayan regions (Sur et al. 2020). The North Eastern Region (NER) of India is lying in the Eastern Himalayas, is highly prone to seismic hazards (seismic zone V), and experiences heavy rainfall. The region has numerous faults, shear zones, and other tectonic features. Together rainfall, high seismicity, and numerous tectonic features make the region highly susceptible to hazard like a landslide.

To reduce the adverse impact of landslides, prepare risk mitigation strategies and plan the infrastructural development accordingly, the landslide susceptibility studies are proven to be an effective tool (Kanungo et al. 2006; Pourghasemi et al. 2012b). The outcome of such studies is in the form of landslide susceptibility maps (LSM) which show the spatial distribution of different susceptibility classes and locations with high risks (Chen and Li 2020). However, the reliability of the LSM depends upon the selected conditioning factors, historical landslides,

quality of data, and the applied methodology for the analysis and modeling (Sarkar and Kanungo 2004). The conditioning factors are the factors associated with topography, geomorphology, geology, land use land cover (LULC), anthropogenic activity, rainfall, seismicity, etc. (Shano et al. 2020) and are responsible for the slope failure. The relation of these factors with the past landslides forms the basis for estimating the future susceptibility of landslide occurrence (Chimidi et al. 2017).

In recent times, with the use of GIS and remote sensing, several landslide susceptibility studies have been carried out worldwide using various methods/models (Sarkar and Kanungo 2004; Yilmaz 2009; Pradhan and Lee 2010; Pourghasemi et al. 2012a,b,c; Shahabi et al. 2014; Jazouli et al. 2019; Sur et al. 2020). The landslide susceptibility models can be divided into qualitative and quantitative approaches (Shano et al. 2020). The qualitative approach includes geomorphic and landslide inventory techniques and an indirect process involving multi-criteria decision analysis (MCDA) methods based on expert judgment for weight evaluation of different thematic data layers (Yilmaz 2009). The most popular MCDA methods are analytical hierarchy process (AHP) and fuzzy set-based analysis (Ercanoglu and Gokceoglu 2004; Kamp et al. 2008; Akgun et al. 2012; Pourghasemi et al. 2012b; Kayastha et al. 2013; Kavzoglu et al. 2014; Shahabi et al. 2014; Shahabi and Hasim 2015; Zhao et al. 2017; Jazouli et al. 2019; Sur et al. 2020). The quantitative approaches include statistical (bivariate or multivariate), deterministic, probabilistic methods, and artificial intelligence-based techniques (artificial neural network, decision trees, support vector machine (SVM), hybrid approaches) (Kanungo et al. 2006; Shano et al. 2020). Among the various quantitative approaches, bivariate statistical methods: frequency ratio (FR), Shannon entropy (SE), the weight of evidence method (WoE); multivariate statistical methods: logistic regression (LR); SVM and ANN are prevalent (Yilmaz 2009; Pradhan and Lee 2010; Pourghasemi et al. 2012b,c; Kavzoglu et al. 2014;

73 Shahabi et al. 2014; Roodposhti et al. 2016; Zaho et al. 2017; Nohani et al. 2019; Pham et al.
74 2019a).

75 In the present study, four models, namely FR, SE, AHP, and Fuzzy-AHP, are utilized to
76 evaluate the landslide susceptibility of the state of Meghalaya. Meghalaya is situated in the
77 NER of India, on the Shillong Plateau of the lesser Himalayas, and is one of the major tourist
78 destinations in NER. There are few landslide susceptibility studies available for western and
79 central Himalayan regions of Lesser and Shivalik Himalayas (Sarkar and Kanungo 2004;
80 Mathew et al. 2009; Pareek et al. 2010; Kayastha et al. 2013; Pham et al. 2019a,b; Sur et al.
81 2020). However, studies of eastern Himalayas are limited. The objective of the present study
82 is to develop the LSM of Meghalaya and identify the major factors governing the landslide
83 occurrence in the area using the four above-mentioned models. Also, to evaluate the prediction
84 power of the most popular bivariate statistical model and MCDA model for the selected study
85 area. The details of the study area, various conditioning factors applied, methodology, and
86 results obtained are discussed in the following sections.

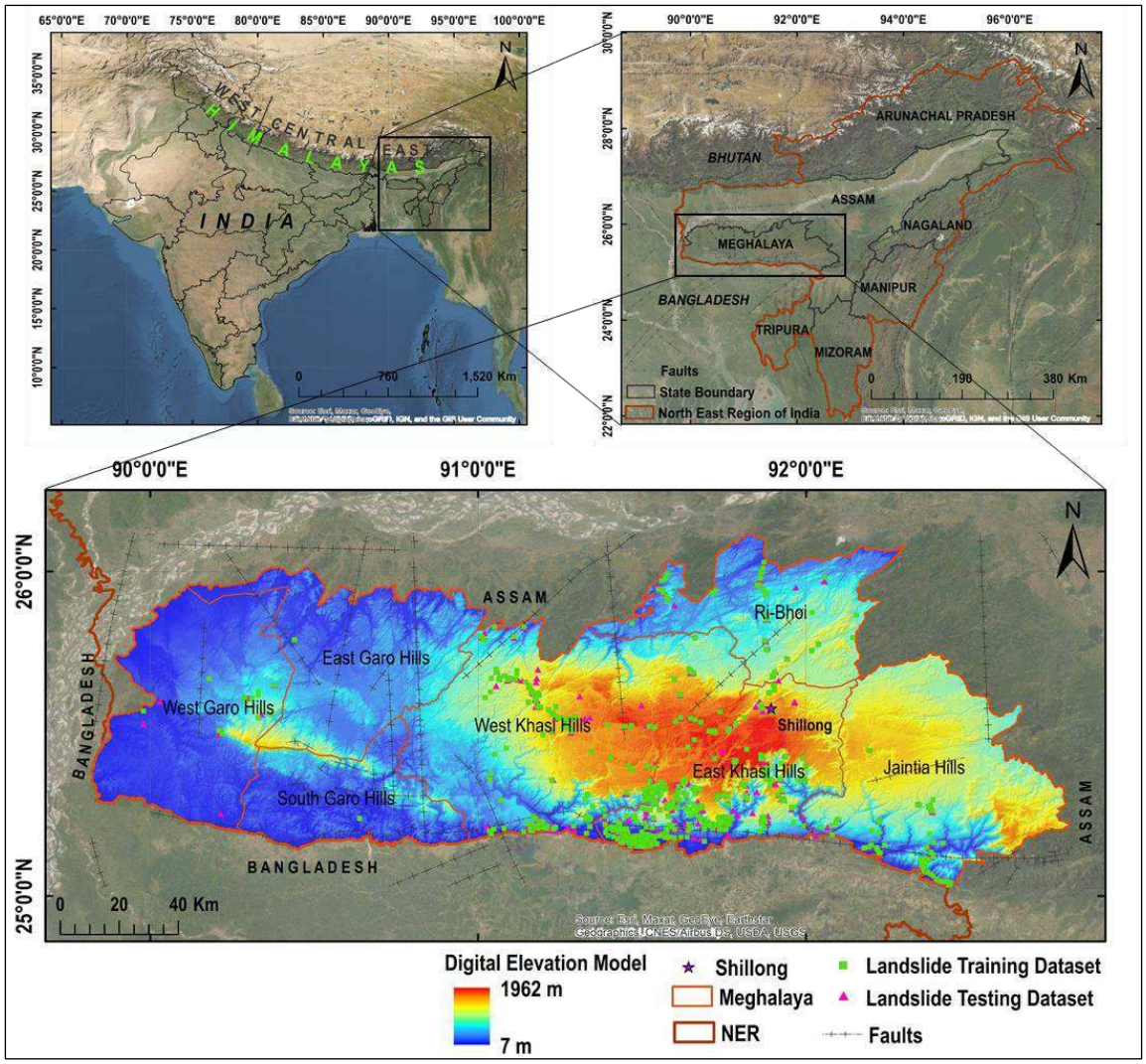

Fig. 1 Study area

2. Description of the study area

The study area is Meghalaya, one of the states of NER India, located on the Shillong Plateau of the Indian Himalayan Region (IHR), covering about 22400 km^2 area (between longitudes 89.821° E to 92.804° E and latitudes 25.031° N to 26.118° N, Fig. 1). It shares its boundary with Assam in the north and east while forming an international border with Bangladesh in the south and west. The elevation of the area ranges from 7 m to 1962 m above mean sea level. Being in the IHR, it is one of the most tectonic-active regions and rainiest places globally (Prokop 2014). The area received an average yearly rainfall of 1234.31 to 7467.48 mm between

1991 and 2020 (30-year period) (Fig. 1). The southern escarpment received the highest rainfall, as high as 12000 mm annual rainfall (recorded in Cherrapunji). The elevation of the southern escarpment of the study area is about 1200-1500 m and is related to the Dauki fault (along the southern boundary), which is much steeper than the northern slope. Due to this sudden rise in elevation over a short distance, the southern escarpment controls rainfall distribution over the region. In the study area, the slope ranges from 0° to 76°.

The study area is covered by various lithologic formations, including Proterozoic (Paleoproterozoic, Mesoproterozoic) (Pr), Late Carboniferous-Permian (LcP), Mesozoic (Jurassic, Cretaceous) (Ms), Paleogene (Oligocene, Eocene, Palaeocene) (Pl), Neogene (Miocene, Pliocene) (Neo) and Cenozoic (Holocene, Quaternary, Meghalyan, Middle-late Pleistocene) (Cn) types of formations (Fig. 2), the details of which are given in Table 1. The region also consists of many lineaments and structural discontinuities and is associated with active tectonics. With respect to land use land cover, most of the study area is covered by dense vegetation (76.06%) followed by light vegetation (17.25%), human settlements and built spaces (3.22%), agricultural land (2.96%), water bodies (0.45%), and rock outcrop and bare lands (0.05%) (Fig. 2 and Table 1). These topological, geological, and other geoenvironmental factors make the study area more prone to disastrous events like landslides.

Table 1 Description of lithological units in the study area

Lithologic Formation	Symbol	Approximate areal coverage (%)
Proterozoic formation (quartz, quartzite with thin phyllite interband, mica gneiss, migmatite, amphibolite, pyroxene granulite, dolerite)	Pr	51

Late carboniferous-Permian (diamictite, phyllite, quartzite, conglomerate, feldspathic sandstone, and carbonaceous shale)	LcP	12.5
Paleogene (shale, sandstone, siltstone, fossiliferous limestone, limestone, phosphatic nodules, fireclay, coal)	Pl	24
Neogene (conglomerate, sandstone, siltstone, mudstone, and marl)	Neo	6.5
Cenozoic (fluvial sediments- sand, silt and clay, loamy sand, pebble, laterite)	Cn	3
Mesozoic (gritty sandstone alternating with conglomerate, basaltic/gabbroic and doleritic dykes, conglomerate, and sandstone with pebbles)	Ms	3

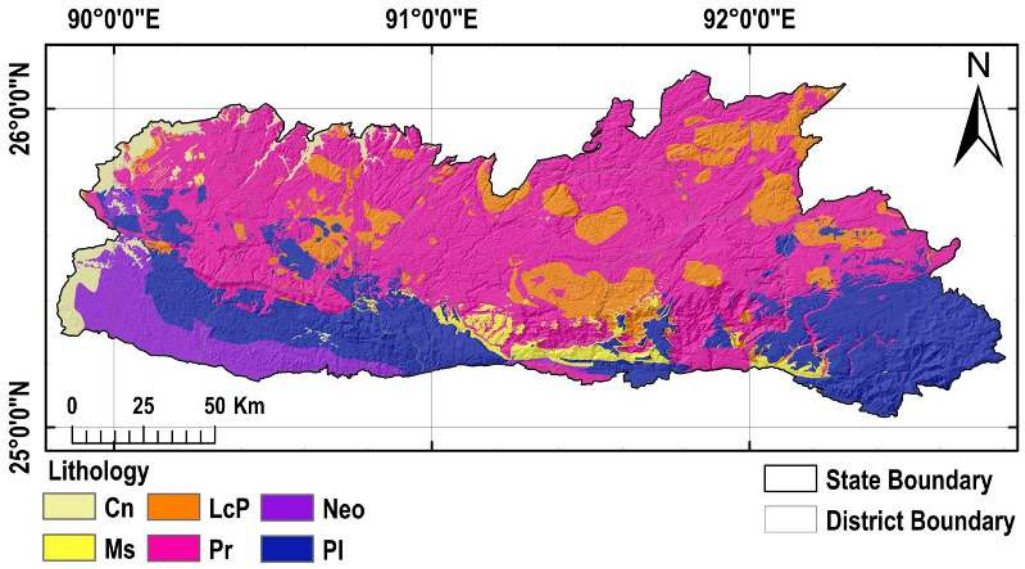

Fig. 2 Lithological units in the study area

3. Material and methods

3.1. Data collection

120 In the present study, the data is collected from several sources such as the Bhukosh-Geological
121 Survey of India (GSI) (https://bhukosh.gsi.gov.in/Bhukosh/MapViewer.aspx) for the creation
122 of landslide inventory, geomorphology map, and maps of other geological features. The USGS
123 earth explorer portal (https://earthexplorer.usgs.gov/) is used to collect the SRTM digital
124 elevation model (DEM) of 30 m resolution. The DEM dataset is utilized to create topographic
125 maps (like slope, aspect, curvature) and to obtain the stream network of the study area.

126 3.1.1. Landslide inventory

127 The prediction accuracy of the LSM primarily depends upon the accuracy of the inventory of
128 the past landslide data (Reichenbach et al. 2018). Landslide data points are collected from the
129 Bhukosh-GSI and Google-Earth images. A sum of 1330 landslides is obtained and mapped to
130 produce the landslide inventory map (Fig. 1). The size of mapped landslides varies from 100
131 m^2 to 1,24,319 m^2. As landslides smaller than one cell size (10 m × 10 m) cannot be drawn, the
132 minimum size is fixed at 100 m^2, and landslides equal to or larger than this size are considered
133 for the study. Identified landslides are generally rainfall-induced and some due to
134 anthropogenic activity. The failure mechanism is either shallow rotational or translational
135 failure with debris and rock-cum-debris movement.

136 Finally, the landslide inventory data are randomly distributed in a 70/30 ratio to create the
137 training and testing dataset, respectively (Chen and Li 2020). The training dataset (at 933
138 locations ≈ 70%) is used to build the model, and the testing dataset (397 sites ≈ 30%) is used
139 to validate the model.

140 3.1.2. Landslide conditioning factor

141 After creating the landslide inventory, selection of factors influencing/governing the landslide,
142 i.e., conditioning factors, are central for any GIS-based landslide susceptibility model (Sarkar
143 and Kanungo 2004). Based on the analysis of previous studies and regional geological-

144 environmental characteristics, fifteen landslide conditioning factors are considered in this
145 study. These factors are discussed in detail in the following section.

146 3.1.2.1. Slope (degrees), aspect, and elevation

147 The slope angles have a direct impact on landslides (Pourghasemi et al. 2012b), as with the
148 increase in the angle of slope, the effect of stress and gravity on the slope forming material
149 increases. The amount of sunshine, rainfall, and other hydrological processes are affected by
150 the slope aspect, which describes the direction of the slope face. It impacts the surface material
151 properties, wetness index, weathering condition, and land cover (Galli et al. 2008). On the other
152 hand, elevation influences landslides indirectly by affecting rainfall, surface forming material,
153 land use/cover, geological, and tectonics (Pham et al. 2019a). Therefore, these factors are
154 frequently used in landslide susceptibility studies (Ercanoglu and Gokceoglu 2004; Sarkar and
155 Kanungo 2004; Mathew et al. 2009; Yilmaz 2009; Pourghasemi et al. 2012a; Chen and Li
156 2020). In this study, the slope map, aspect map, and elevation map of the study area are derived
157 from DEM using ArcMap 10.8, resampled to 10 m resolution (Figs. 3a-c).

158 3.1.2.2. Plan curvature

159 The plan curvature is derived from DEM using ArcMap 10.8 with a resolution of 10 m.
160 Curvature influences the surface erosion processes, especially during the rainfall, by either
161 converging or diverging the downhill flow and thus becomes one of the critical factors
162 controlling the landslide event (Oh and Pradhan 2011). The plan curvature classified into three
163 classes (concave (<-0.05), flat (-0.05-0.05), and convex (>0.05)) (Fig. 3d).

164 3.1.2.3. Stream power index (SPI) and topographic wetness index (TWI)

165 Stream power index (SPI) is a topographic factor that reflects the erosive power of streams in
166 any catchment assuming the discharge is proportional to a specific catchment area (A_S) (Moore
167 et al. 1991). The SPI can be obtained using Equation 1 (Moore et al. 1991).

168 $$SPI = A_S \times \tan\beta \quad (1)$$

169 Where β is the local slope (in degrees).

170 Topographic wetness index (TWI) is another topographic factor frequently used in landslide
171 susceptibility studies, suggesting the tendency of water to accumulate at any point in the
172 catchment and the tendency of movement of water along the slope under gravitational forces
173 (Bordoni et al. 2020). Water accumulation at any point can affect the stability of the slope,
174 depending on the surface forming material and its effect on the geotechnical properties like
175 permeability, pore water pressure, and shear strength (Yilmaz 2009). It can be defined by
176 Equation 2.

177 $$TWI = \ln\left(\frac{a}{\tan\beta}\right) \quad (2)$$

178 Where a is upslope catchment area, and $tan(\beta)$ is the slope angle.

179 The present study prepared the SPI and TWI map using SAGA GIS tools in QGIS and classified
180 it into five classes, as shown in Figs. 3e-f.

181 3.1.2.4. Distance from the river

182 Distance from the river is inversely related to landslides, as the closer the river the more the
183 chance of the slope being unstable. The proximity to streams increases the soil moisture and
184 erodes the toe of the slope, making the area in the vicinity more susceptible to landslides
185 (Pourghasemi et al. 2012b). The stream network map of order four or more is obtained by using
186 DEM in ArcMap. Finally, the area is divided into five different buffer zones from the river at
187 a 150 m distance (Fig. 3g).

188 3.1.2.5. Distance from road

189 An anthropogenic activity like road construction alters the natural slope of the hilly area and
190 increases the slope instability. In the past, numerous landslides have occurred in the vicinity of
191 roads either constructed or under construction (Wang et al. 2015; Roodposhti et al. 2016; Pham
192 et al. 2019b). In the present study, the road network data is collected from the Openstreet map
193 (https://www.openstreetmap.org/export). In this study, highways, primary, secondary, and
194 tertiary roads are considered. Finally, the area is divided into five different buffer zones from
195 the roads at a 150 m distance (Fig. 3h).

196 3.1.2.6. Distance from fault

197 Fault represents structural discontinuities with reduced rock strength, making the area
198 vulnerable to landslides (Chen and Li 2020). In this study, major structural discontinuities are
199 obtained from Bhukosh-GSI and buffered into five different zones at 1000 m distance intervals
200 (Fig. 3i).

201 3.1.2.7. Land use land cover (LULC)

202 The land use land cover (LULC) of any region has a direct influence on slope stability. The
203 bare land and built space have shown a positive impact of landslides in the past. In the present
204 study, a global LULC map derived from Sentinet-2 imagery at 10 m resolution by ESRI is
205 used. The map is available with ten land use classes: water, trees (forested area/dense
206 vegetation), grass, flooded vegetation, crops, shrub, built space, bare ground snow/ice, and
207 clouds. The LULC map is extracted by mask for the study area, and classes like grass and shrub
208 are grouped into a single category named light vegetation. In contrast, flooded vegetation and
209 crop are grouped into agricultural land (Fig. 3j). Further, the accuracy assessment of
210 reclassified LULC map is done through randomly generated 300 points falling under different
211 land-use classes (Table 2). The overall accuracy is 85.33%, while the kappa coefficient (k)
212 value is 0.824. The value of $k > 0.8$ shows that the used map is reasonably accurate.

Table 2 Accuracy assessment of LULC map using kappa coefficient (*k*)

LULC Classes		Water	Dense veg.	Light veg.	Agri land	Built space	Bare land	Total (User)
		1	**2**	**3**	**4**	**7**	**8**	
Water	1	49	0	0	1	0	0	50
Dense veg.	2	0	43	5	1	0	1	50
Light veg.	3	0	1	35	10	0	4	50
Agri land	4	1	0	5	41	0	3	50
Built space	7	0	2	4	3	41	0	50
Bare land	8	2	0	1	0	0	47	50
Total (Producer)		52	46	50	56	41	55	300
Overall accuracy								**85.33%**
kappa coefficient(*k*)								**0.82**

3.1.2.8. Normalized difference vegetation index

Normalized difference vegetation index (NDVI) is an indicator of green cover over an area and the health of the biomass. Higher NDVI values indicate more vegetation cover, and a healthy vegetation cover offers higher stability to slopes and reduces the probability of landslide (Nohani et al. 2019). The NDVI map is derived using Sentinel-2 multispectral imagery with 10 m resolution using ArcMap 10.8 and grouped into six classes (Fig. 3k).

3.1.2.9. Rainfall

Precipitation, especially in the form of rain, is one of the foremost reasons for landslide occurrence on hill slopes. However, the influence of rainfall on landslides is governed by the slope forming material, land cover, lithology, etc. (Can et al. 2005). For this study, rainfall data of the last 30 years (1991-2020) is collected from the India Meteorological Department (Pai et al. 2014) (https://www.imdpune.gov.in/Clim_Pred_LRF_New/Grided_Data_Download.html). The mean annual rainfall (1991-2020) is calculated and mapped in the GIS environment (Fig. 3l).

3.1.2.10. Soil texture

230 The topsoil covers of any area influence the landslide susceptibility (Sarkar and Kanungo
231 2004). In the present study, the soil map is derived from a world soil map (FAO soil map). The
232 soil present in the area is mostly loam, sandy loam, and clay (Fig. 3m).

233 3.1.2.11. Geomorphology

234 The geomorphology of an area influences the landslide occurrence in the area and is considered
235 in many susceptibility studies (Pham et al. 2019b). A geomorphological map for the study area
236 is obtained from the Bhukosh-GSI and the region is classified into seven geomorphological
237 units (highly dissected plateau (HDP), moderate to low dissected plateau (MDP), highly
238 dissected hills and valley (HDHV), moderate to low dissected hills and valley (MDHV),
239 pediment-pediplain complex (PC), alluvial-flood plain (AP) and water bodies (W)) (Fig. 3n).

240 3.1.2.12. Lithology

241 The lithology of an area often governs the rock strength and permeability of the rocky soils.
242 Therefore, in landslide susceptibility studies, it is considered one of the essential factors
243 (Pradhan and Lee 2010; Wang et al. 2015; Chen and Li 2020). The lithological map of the
244 study area is obtained from Bhukosh-GSI (at a scale of 1:2M). The lithological formations are
245 grouped into six classes depending upon the geological era, as mentioned in section 2 (Fig. 2).

246 All fifteen landslide conditioning factors are transformed into the spatial resolution of 10 m
247 before using for the susceptibility studies.

248

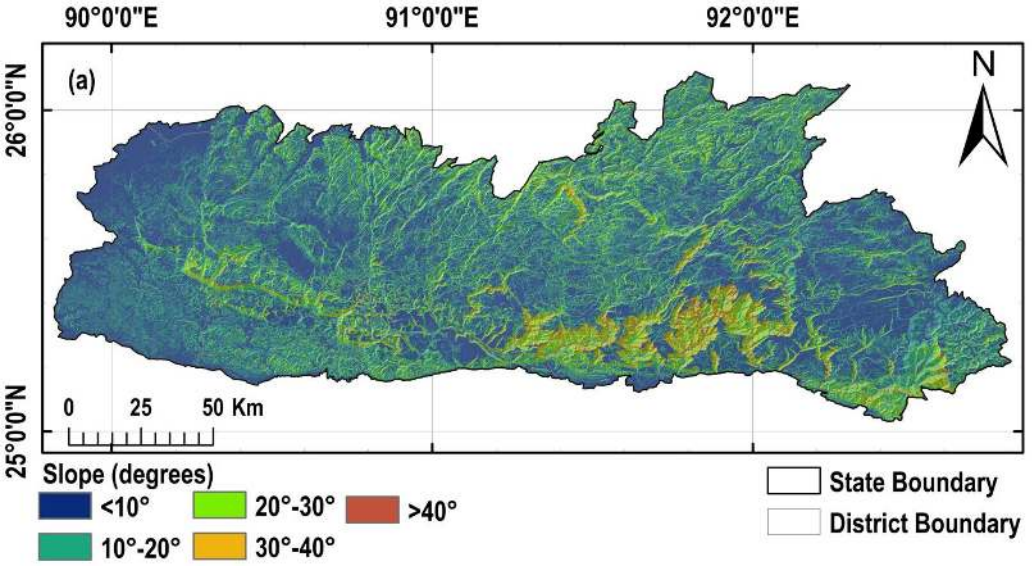
90°0'0"E
91°0'0"E
92°0'0"E
26°0'0"N
25°0'0"N
(a)
N
0 25 50 Km
Slope (degrees)
<10°
10°-20°
20°-30°
30°-40°
>40°
State Boundary
District Boundary

249

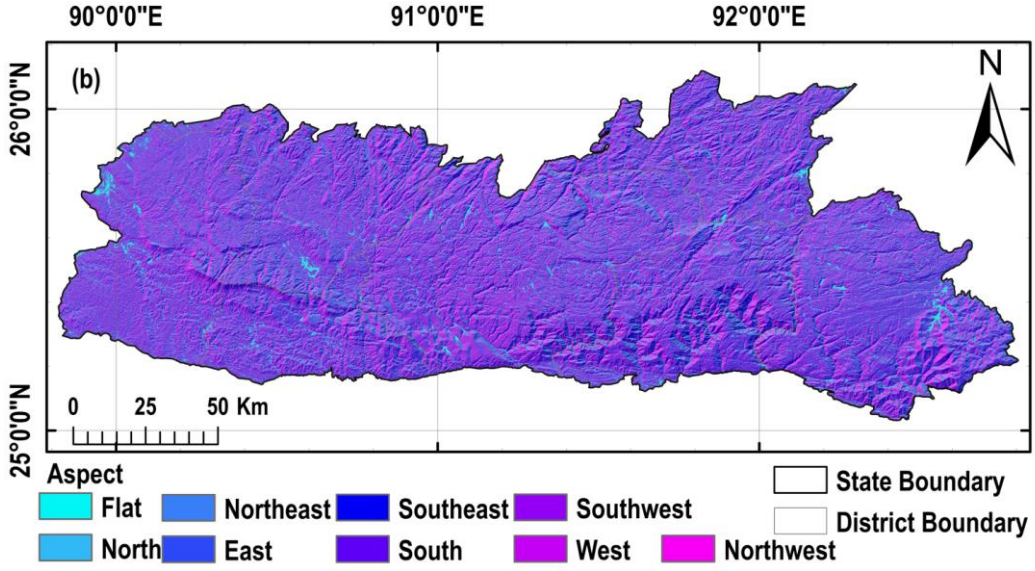
90°0'0"E
91°0'0"E
92°0'0"E
26°0'0"N
25°0'0"N
(b)
N
0 25 50 Km
Aspect
Flat
North
Northeast
East
Southeast
South
Southwest
West
Northwest
State Boundary
District Boundary

250

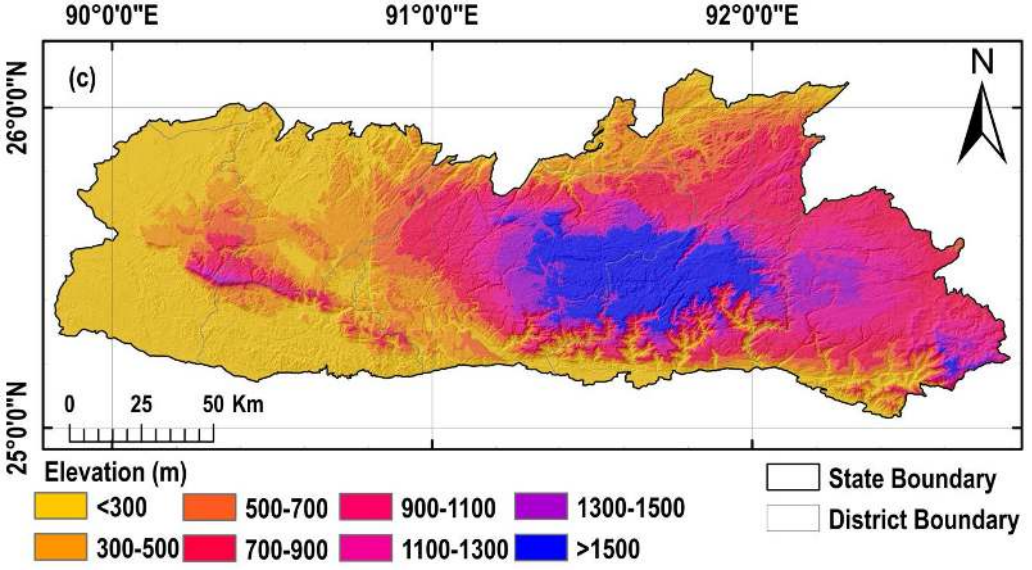
90°0'0"E
91°0'0"E
92°0'0"E
26°0'0"N
25°0'0"N
(c)
N
0 25 50 Km
Elevation (m)
<300
300-500
500-700
700-900
900-1100
1100-1300
1300-1500
>1500
State Boundary
District Boundary

251

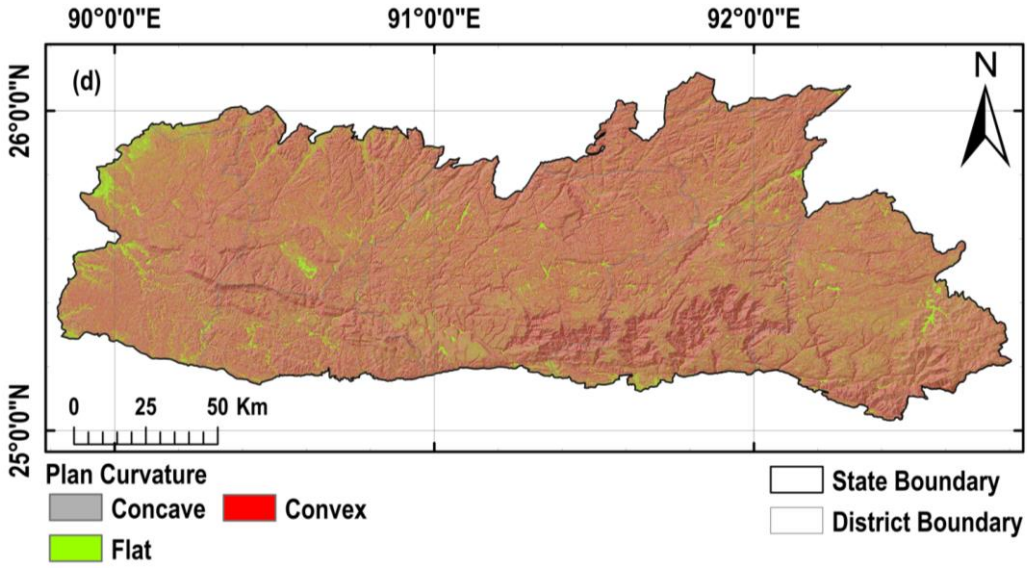
90°0'0"E
91°0'0"E
92°0'0"E
26°0'0"N
25°0'0"N
(d)
N
0 25 50 Km
Plan Curvature
Concave
Convex
Flat
State Boundary
District Boundary

252

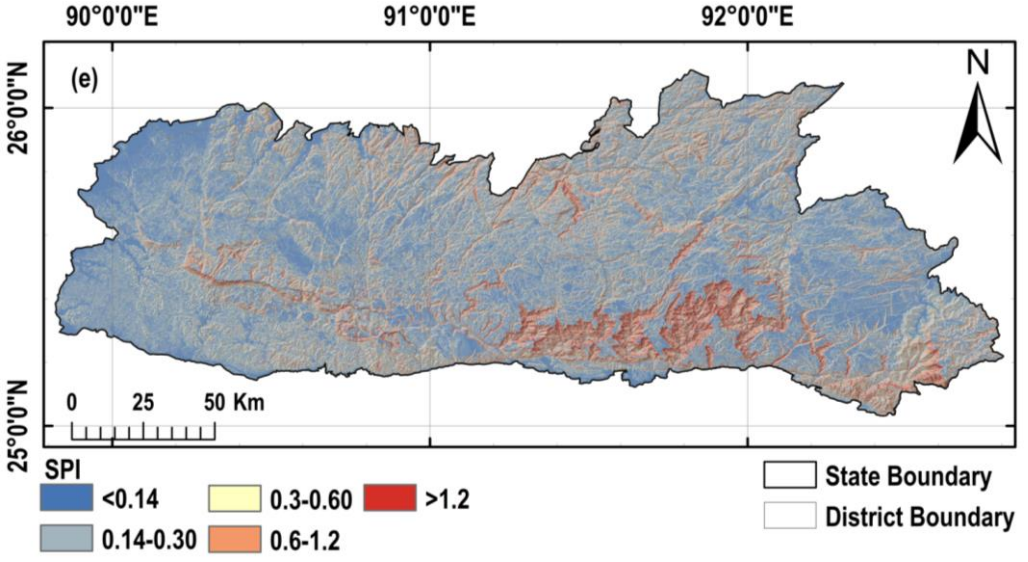
90°0'0"E
91°0'0"E
92°0'0"E
26°0'0"N
25°0'0"N
(e)
N
0 25 50 Km
SPI
<0.14
0.14-0.30
0.3-0.60
0.6-1.2
>1.2
State Boundary
District Boundary

253

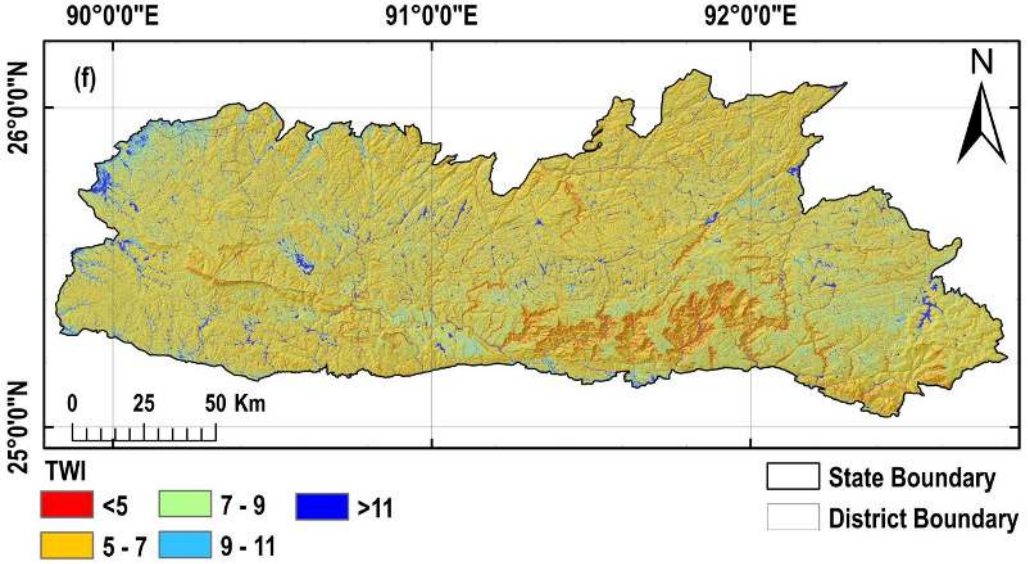
90°0'0"E
91°0'0"E
92°0'0"E
26°0'0"N
25°0'0"N
(f)
N
0 25 50 Km
TWI
<5
5 - 7
7 - 9
9 - 11
>11
State Boundary
District Boundary

254

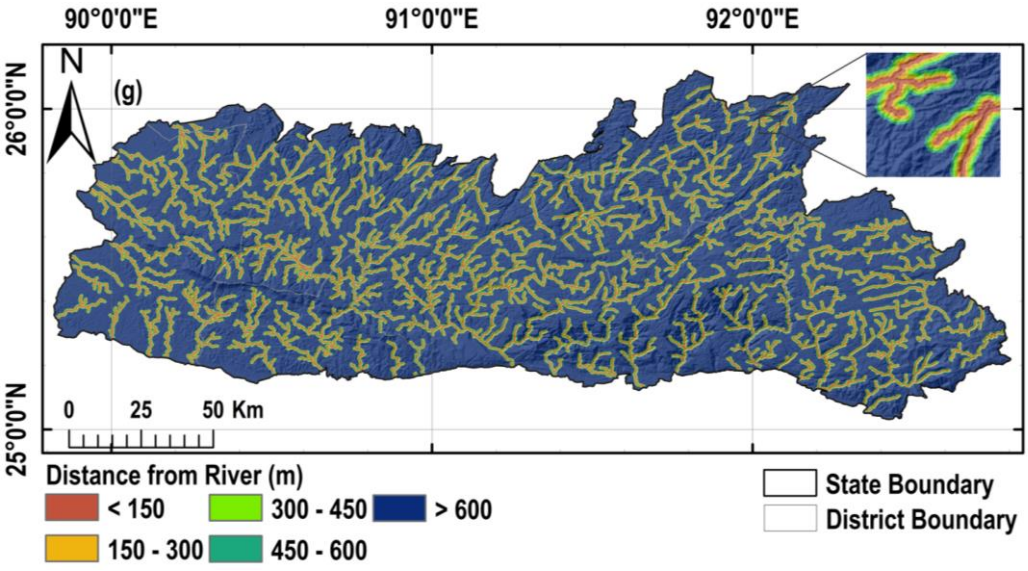
90°0'0"E
91°0'0"E
92°0'0"E
N
(g)
26°0'0"N
25°0'0"N
0 25 50 Km
Distance from River (m)
< 150
300 - 450
> 600
150 - 300
450 - 600
State Boundary
District Boundary

255

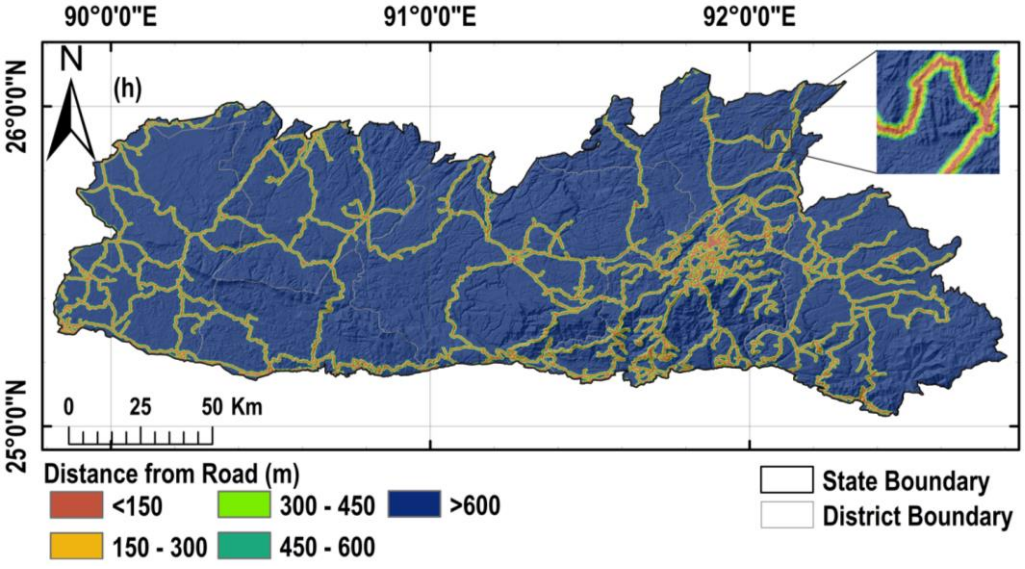
90°0'0"E
91°0'0"E
92°0'0"E
N
(h)
26°0'0"N
25°0'0"N
0 25 50 Km
Distance from Road (m)
<150
300 - 450
>600
150 - 300
450 - 600
State Boundary
District Boundary

256

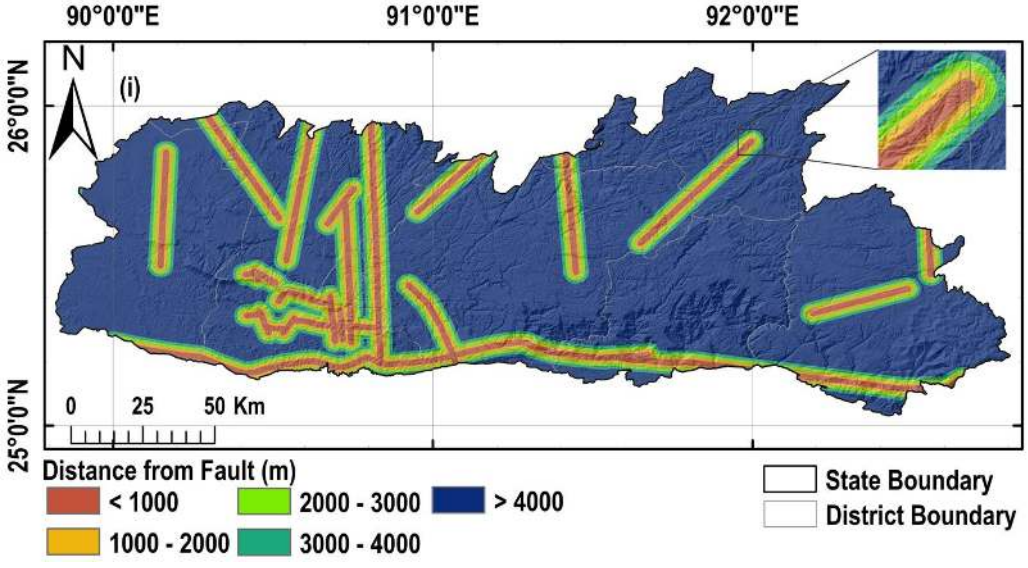
90°0'0"E
91°0'0"E
92°0'0"E
N
(i)
26°0'0"N
25°0'0"N
0 25 50 Km
Distance from Fault (m)
< 1000
2000 - 3000
> 4000
1000 - 2000
3000 - 4000
State Boundary
District Boundary

257

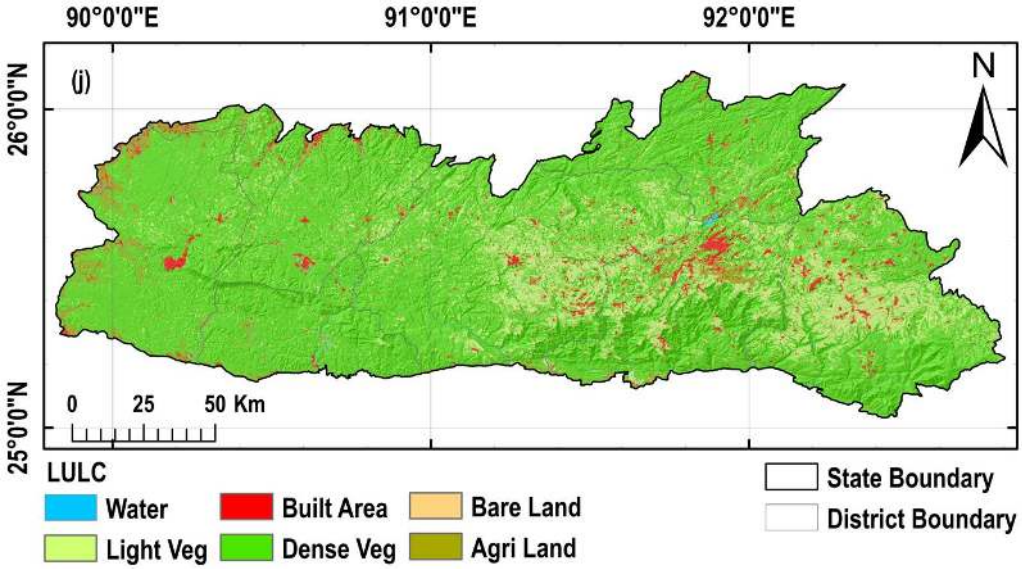
90°0'0"E
91°0'0"E
92°0'0"E
26°0'0"N
25°0'0"N
(j)
N
0 25 50 Km
LULC
Water
Built Area
Bare Land
Light Veg
Dense Veg
Agri Land
State Boundary
District Boundary

258

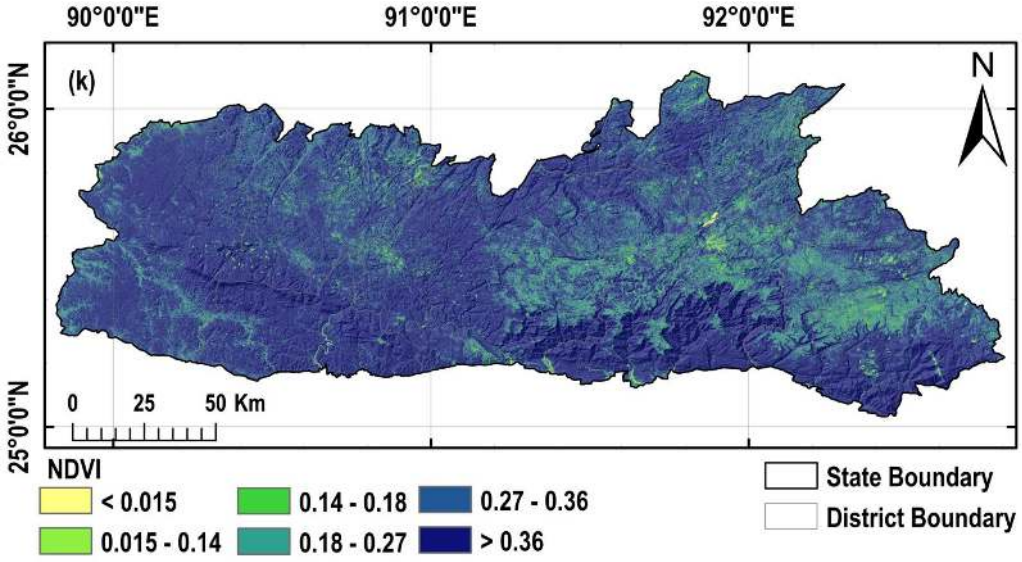
90°0'0"E
91°0'0"E
92°0'0"E
26°0'0"N
25°0'0"N
(k)
N
0 25 50 Km
NDVI
< 0.015
0.015 - 0.14
0.14 - 0.18
0.18 - 0.27
0.27 - 0.36
> 0.36
State Boundary
District Boundary

259

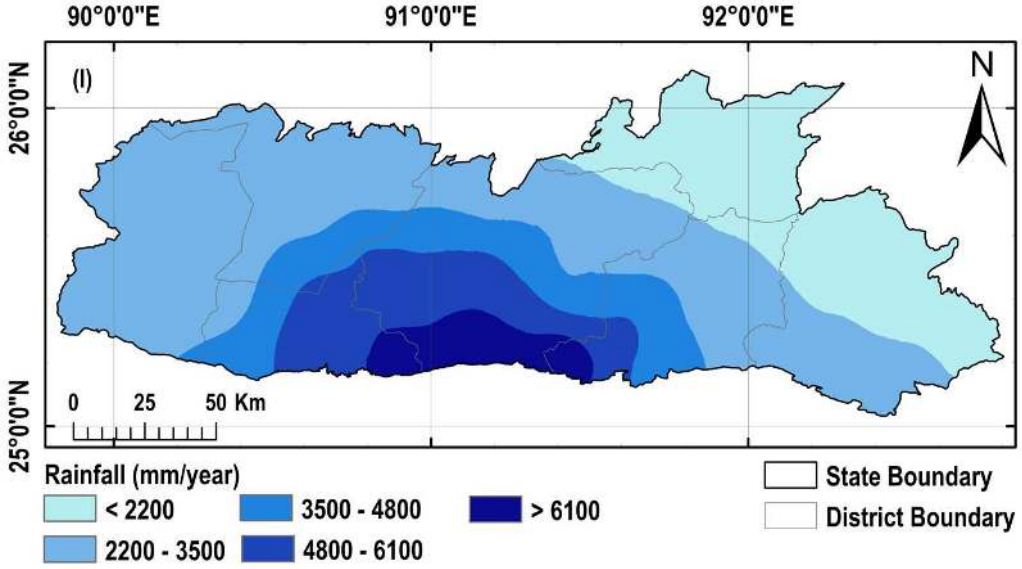
90°0'0"E
91°0'0"E
92°0'0"E
26°0'0"N
25°0'0"N
(l)
N
0 25 50 Km
Rainfall (mm/year)
< 2200
2200 - 3500
3500 - 4800
4800 - 6100
> 6100
State Boundary
District Boundary

260

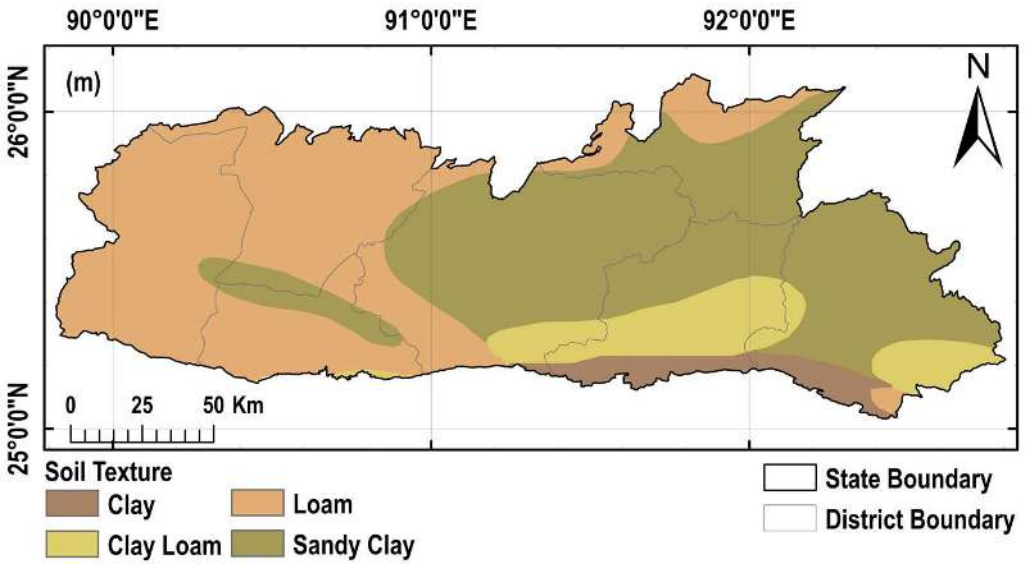

261

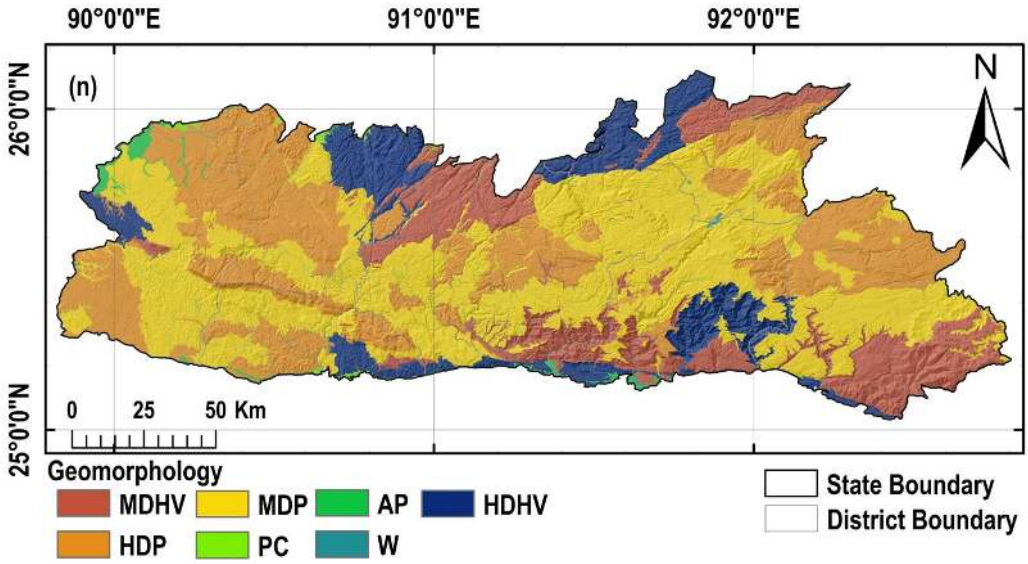

262

263 **Fig. 3** Conditioning factor maps of the study area: (a) Slope (degrees), (b) Aspect of slope, (c)
264 Elevation, (d) Plan Curvature, (e) SPI, (f) TWI, (g) Distance from river, (h) Distance from road,
265 (i) Distance from faults, (j) LULC, (k), NDVI, (l) mean annual rainfall (mm/year), (m) Soil
266 texture, (n) Geomorphology.

267 **3.2. Methodology**

268 For landslide susceptibility assessment, the present study utilizes the bivariate models
269 (frequency ratio and Shannon entropy) and MCDA models (AHP and Fuzzy-AHP), elaborated
270 in the following section.

3.2.1. Frequency ratio (FR)

This approach suggests the possibility of a future event based on past information and it is used in various studies (Yilmaz 2009; Pradhan and Lee 2010; Chimidi et al. 2017; Nohani et al. 2019; Shano et al. 2020). This method derives the spatial relation between landslide location (number of landslide pixels) and each landslide conditioning factor. As it represents the possibility of occurrence, the greater FR value shows higher chances of landslide occurrence and higher corresponding hazard (Pradhan and Lee 2010). FR of each class of all the conditioning factors can be obtained using Equation 3.

$$FR_i = \frac{(LS_i / LS)}{(A_i / A)} \tag{3}$$

Where FR_i = frequency ratio of i^{th} class, LS_i = total landslide area (number of landslide pixels) in the i^{th} class, LS = total landslide area (total number of landslide pixels) in the study area, A_i = area falling under i^{th} class (total number of pixels of i^{th} class), and A = total area (total number of pixels of the entire map).

These FR values of different classes (Table 5) are then used to obtain the prediction rate (PR) of each factor which depicts the weightage of individual factors, using Equations 4-6.

$$RF_i = \left(FR_i / \sum FR \right) \tag{4}$$

$$R_j = MAX(RF_{i,j}) - MIN(RF_{i,j}) \tag{5}$$

$$PR_j = R_j / MIN(R) \tag{6}$$

Where RF is relative frequency, $MAX(RF_{i,j})$ is the maximum value of RF of j^{th} factor, $MIN(RF_{i,j})$ is the minimum value of RF of j^{th} factor, PR_j is the prediction rate of j^{th} factor.

The PR_j will be the weight of the j^{th} factor, i.e., $W_{j,FR}$. Finally, to obtain the landslide susceptibility map, the *FR* of different classes of influencing parameters and $W_{j,FR}$ of each parameter is integrated and summed up together, as in Equation 7 (Yilmaz 2009).

$$LSM_{FR} = \sum_{j=1}^{n}\sum_{i=1}^{m}\left(FR_{ij} \times W_{j,FR}\right) \tag{7}$$

3.2.2. Shannon entropy (SE)

Entropy is the quantitative measurement of deviation, variability, instability, and uncertainty of a system and can be used to predict the future trend of a specified system (Lotfi and Fallahnejad 2010). The Shannon entropy has been widely used for the weighted index calculation in the landslide and other hazard studies (Wang et al. 2011; Pourghasemi et al. 2012c; Zhao et al. 2017; Nohani et al. 2019). It analyses the dissimilarity in the system in susceptibility studies, demonstrating the potential for each contributing factor to cause a landslide. A higher SE index indicates a more significant impact of the factor on the landslide occurrence (Roodposhti et al. 2016). Equations 8-10 are used for the calculation of information coefficient (weighted index) based on SE (Pourghasemi et al. 2012c; Zhao et al. 2017).

$$P_{ij} = FR_{ij} \Big/ \sum_{i=1}^{m} FR_{ij} \tag{8}$$

$$D_j = \left(\frac{-1}{\log_2(m_j)}\right)\sum_{i=1}^{m} P_{ij}\log_2 P_{ij} \quad , \quad i = 1, 2\ldots m \text{ and } j = 1, 2\ldots n \tag{9}$$

$$W_{j,SE} = \left(1 - D_j\right) \Big/ \sum_{j=1}^{n}\left(1 - E_j\right) \tag{10}$$

Where *FR* = frequency ratio, P_{ij} = probability density for each class, D_j = entropy of the j^{th} conditioning factor, m_j = number of classes in the j^{th} factor, *n* = number of factors, and $W_{j,SE}$ =

entropy weight of each factor. Table 5 shows entropy weights obtained for all the conditioning factors. These are normalized and used to get the LSM shown in Fig. 6.

3.2.3. Analytical hierarchy process (AHP)

It is a semi-quantitative, multi-criteria decision-making approach developed by Saaty (Saaty 2000,2008). It involves problem definition, objective, alternatives, pairwise comparison matrix for weight determination, and overall priority of the factors (or sub-factors) contributing to landslide (Saaty 2008; Shano et al. 2020). In landslide susceptibility studies, it is one of the frequently used methods for assigning the weightage to conditioning factors and sub-factors (Kamp et al. 2008; Kayastha et al. 2013; Shahabi and Hasim 2015; Jazouli et al. 2019).

In AHP, conditioning factors (or their classes) are arranged in the hierarchic order and assigned a numerical value subjective to judgment based on their relative importance, forming a pairwise comparison matrix (Table 6 and 7). In the matrix, the scale of assigned value can vary between 1 and 9 based on degrees of preference of one factor (on the vertical axis) over the other (on the horizontal axis) (Table 3). A higher value shows greater dominance of that factor. Similarly, these values can vary inversely (1/9 to 1) when the element on the horizontal axis is more dominant than that on a vertical axis (Table 3). In the present study, for assigning the degree of preference scale to a factor (or their classes), the relative percentage of area affected by landslide in that class category is used to make the judgment. Thus, it allows the consideration of "previous knowledge" and reduces the bias in the scheme (Yilmaz 2009). After the comparison matrix is built up, the next step is to find criteria weights and consistency ratio (CR) in Equation 11.

$$CR = CI/RI \tag{11}$$

$$CI = \left(\lambda_{\max} - 1\right)/\left(n - 1\right) \tag{12}$$

Where CI = consistency index, λ_{max} = principal Eigenvalue, and n = order of the matrix. And RI = random consistency index that depends upon the order of the matrix (Table 4).

As per Saaty (2008), CR should be less than 0.10, only then the formed comparison matrix is consistent, and if not so, it represents inconsistency in the factor ratings. One must revise the matrix until it becomes consistent. In the present study, for the pairwise comparison matrix of conditioning factors, the CR is equal to 0.049. Also, for the comparison matrix of classes of each factor, the CR value is less than 0.10 (Table 6 and 7).

Finally, the criteria weights can be integrated to generate the LSM using Equation 13.

$$LSM_{AHP} = \sum_{j=1}^{n}\sum_{i=1}^{m}(w_{ij,AHP} \times W_{j,AHP}) \quad (13)$$

Where $W_{j,AHP}$ = weight of j^{th} conditioning factors and $w_{ij,AHP}$ = weight of an i^{th} class of the j^{th} factor using AHP. Fig. 8 shows the LSM using this model.

Table 3 The scale of preference in AHP (Saaty 2000) and triangular fuzzy scale in FAHP (Kannan et al. 2013)

Degree of preference (AHP)/ Linguistic Variables (FAHP)	**The scale of preferences (Saaty, 2000)**	**Triangular Fuzzy Scale of preference (Kannan et al. 2013)**
Equal	1	1,1,1
Moderate	3	2,3,4
Strong	5	4,5,7
Very strong	7	6,7,8
Extremely strong	9	9,9,9
Intermediate	2	1,2,3
	4	3,4,5
	6	5,6,7
	8	7,8,9
Reciprocals	1/2, 1/3, ..., 1/9	Inverse (e.g. $(2,3,4)^{-1}$ = (1/4,1/3,1/2))

Table 4 Random consistency index as per Saaty (2000)

n	1	2	3	4	5	6	7	8	9	10	11	12	13
RI	0.00	0.00	0.58	1.12	1.24	1.32	1.41	1.45	1.49	1.51	1.53	1.56	1.57

348

349 **Table 5** Frequency ratio of classes of various conditioning factors and weights assigned using FR and SE models

Sl. No	Conditioning Factors	Class	Pixels (%)	Landslide Pixels (%)	FR	PR ($W_{j,FR}$)	$W_{i,SE}$
1	Slope (degrees)	<10°	48.70	4.31	0.08	4.79	11.45
		10°-20°	34.11	17.58	0.51		
		20° - 30°	12.43	29.11	2.34		
		30° - 40°	3.91	33.04	8.45		
		>40°	0.85	15.95	18.69		
2	Aspect	Flat (-1)	1.77	0.00	0.00	1.27	1.73
		North (0-22.5, 337.7-360)	6.37	5.04	0.79		
		Northeast (22.5-67.5)	10.59	14.05	1.32		
		East (67.5-112.5)	12.93	14.51	1.12		
		Southeast (112.5-157.5)	14.98	16.50	1.10		
		South (157.5-202.5)	14.75	16.86	1.14		
		Southwest (202.5-247.5)	13.18	14.65	1.11		
		West (247.5-292.5)	12.99	8.81	0.67		
		Northwest (292.5-337.5)	12.45	9.59	0.77		
3	Elevation (m)	<300	29.73	28.00	0.94	1.00	0.71
		300 - 500	15.60	12.89	0.82		
		500 - 700	10.75	11.87	1.10		
		700 - 900	11.46	9.42	0.82		
		900 - 1100	10.13	8.77	0.86		
		1100 - 1300	8.09	12.40	1.53		
		1300 - 1500	6.35	11.31	1.78		
		>1500	7.90	5.34	0.67		
4	Plan curvature (100/m)	Concave (<-0.05)	35.83	51.13	1.42	2.74	2.47
		Flat (-0.05-0.05)	21.52	9.43	0.43		
		Convex (>0.05	42.65	39.43	0.92		
5		<150	8.35	4.02	0.48	1.15	0.53

	Distance from river (m)	150 - 300	7.80	6.93	0.88		
		300 - 450	7.37	6.10	0.82		
		450 - 600	7.02	6.22	0.88		
		>600	69.46	76.73	1.10		
6	Distance from road (m)	<150	5.97	22.06	3.69	2.44	2.43
		150 - 300	5.12	7.50	1.46		
		300 - 450	4.62	10.88	2.35		
		450 - 600	4.24	6.00	1.41		
		>600	80.06	53.56	0.66		
7	Distance from faults (m)	<1000	7.27	5.02	0.69	1.50	1.39
		1000 - 2000	7.09	6.99	0.98		
		2000 - 3000	7.00	13.36	1.90		
		3000 - 4000	6.79	12.38	1.82		
		>4000	71.86	62.27	0.86		
8	LULC	Waterbodies	0.45	0.35	0.77	5.45	11.84
		Dense Vegetation	76.06	79.89	1.05		
		Light Vegetation	17.25	16.95	0.98		
		Agricultural Land	2.96	0.05	0.01		
		Built Area	3.22	2.35	0.73		
		Bare Land	0.05	0.42	8.48		
9	NDVI	<0.015	0.08	0.01	0.07	2.16	2.92
		0.015 - 0.14	1.24	2.52	2.02		
		0.14 - 0.18	2.32	4.13	1.78		
		0.18 - 0.27	12.90	15.24	1.18		
		0.27 - 0.36	20.12	20.63	1.02		
		0.36 - 0.999	63.33	57.48	0.90		
10	SPI	< 0.13523	44.64	13.34	0.29	5.05	10.94
		0.13523 - 0.3	21.29	8.93	0.41		
		0.3 - 0.6	19.05	16.26	0.85		
		0.6 - 1.2	11.26	28.92	2.56		

		>1.2	3.76	32.55	8.65		
11	TWI	<5	2.14	16.27	7.58	5.92	14.01
		05-07.0	61.77	68.4	1.10		
		07-09.0	23.59	11.80	0.50		
		09-11.0	6.70	2.69	0.40		
		>11	5.77	0.82	0.14		
12	Rainfall (mm/year)	<2200	23.14	5.66	0.24	4.17	7.28
		2200 - 3500	47.01	27.14	0.57		
		3500 - 4800	13.39	16.26	1.21		
		4800 - 6100	11.65	24.98	2.14		
		>6100	4.79	25.93	5.41		
13	Soil texture	Loam	41.33	13.80	0.33	4.14	10.25
		Sandy Clay	44.40	10.11	0.22		
		Clay Loam	10.26	49.46	4.81		
		Clay	3.99	26.62	6.67		
14	Geomorphology	MDHV	14.26	38.12	2.67	3.16	9.37
		HDP	30.07	3.10	0.10		
		MDP	40.50	14.80	0.36		
		PC	0.28	0	0.00		
		AP	0.96	0.02	0.02		
		W	2.53	4.63	1.82		
		HDHV	11.38	39.30	3.45		
15	Lithology	Cn	3.15	0.01	0.00	5.53	12.67
		Neo	6.46	2.73	0.42		
		Pl	24.09	34.09	1.41		
		Ms	2.93	22.99	7.84		
		LcP	12.30	8.00	0.65		
		Pr	51.05	32.15	0.63		

350

351 **Table 6** Pairwise comparison matrix, consistency ratio, and weights assigned to each class of different conditioning factors by AHP

Conditioning factors	Classes		1	2	3	4	5	6	7	8	9	CR	Weights ($w_{ij,AHP}$)
Slope (degree)	<10°	**1**	1	0.50	0.33	0.20	0.14					0.017	0.052
	10°-20°	**2**		1	0.50	0.33	0.20						0.087
	20° - 30°	**3**			1	0.50	0.33						0.150
	30° - 40°	**4**				1	0.33						0.239
	>40°	**5**					1						0.471
Aspect	Flat (-1)	**1**	1	0.11	0.11	0.13	0.13	0.13	0.13	0.14	0.14	0.054	0.014
	North (0-22.5)	**2**		1	1	2	3	3	4	5	4		0.235
	Northeast (22.5-67.5)	**3**			1	2	2	3	2	3	3		0.193
	East (67.5-112.5)	**4**				1	1	2	2	6	7		0.159
	Southeast (112.5-157.5)	**5**					1	1	2	5	3		0.123
	South (157.5-202.5)	**6**						1	1	3	3		0.095
	Southwest (202.5-247.5)	**7**							1	3	2		0.085
	West (247.5-292.5)	**8**								1	0.50		0.043
	Northwest (292.5-337.5)	**9**									1		0.053
Elevation (m)	<300	**1**	1	1	0.50	0.50	0.20	0.20	0.20	0.33		0.031	0.040
	300 - 500	**2**		1	0.33	0.50	0.33	0.25	0.25	0.33			0.044
	500 - 700	**3**			1	1	0.25	0.25	0.20	0.50			0.071
	700 - 900	**4**				1	0.50	0.33	0.33	0.33			0.072
	900 - 1100	**5**					1	1	0.50	0.50			0.159
	1100 - 1300	**6**						1	1	2			0.217
	1300 - 1500	**7**							1	2			0.241
	>1500	**8**								1			0.156
Plan curvature (100/m)	Concave (<-0.05)	**1**	1	4	1							0.000	0.444
	Flat (-0.05-0.05)	**2**		1	0.25								0.111

	Convex (>0.05)	**3**			1					0.444
Distance from river (m)	<150	**1**	1	0.50	2	2	3		0.020	0.247
	150 - 300	**2**		1	2	3	4			0.370
	300 - 450	**3**			1	2	3			0.189
	450 - 600	**4**				1	2			0.120
	>600	**5**					1			0.073
Distance from road (m)	<150	**1**	1	2	3	4	5		0.015	0.416
	150 - 300	**2**		1	2	3	4			0.262
	300 - 450	**3**			1	2	3			0.161
	450 - 600	**4**				1	2			0.099
	>600	**5**					1			0.062
Distance from faults (m)	<1000	**1**	1	1	2	2	3		0.020	0.292
	1000 - 2000	**2**		1	1	3	4			0.289
	2000 - 3000	**3**			1	2	3			0.220
	3000 - 4000	**4**				1	2			0.124
	>4000	**5**					1			0.075
LULC	Waterbodies	**1**	1	0.50	0.25	0.50	0.20	0.17	0.047	0.046
	Dense Vegetation	**2**		1	0.33	0.33	0.33	0.20		0.065
	Light Vegetation	**3**			1	2	2	0.33		0.199
	Agricultural Land	**4**				1	0.33	0.25		0.106
	Built Area	**5**					1	0.33		0.184
	Bare Land	**6**						1		0.401
NDVI	<0.015	**1**	1	0.17	0.17	0.33	0.33	0.50	0.028	0.045
	0.015 - 0.14	**2**		1	0.50	2	3	4		0.266
	0.14 - 0.18	**3**			1	2	3	4		0.335
	0.18 - 0.27	**4**				1	2	3		0.167
	0.27 - 0.36	**5**					1	3		0.120
	0.36 - 0.999	**6**						1		0.066
SPI	< 0.13523	**1**	1	0.50	0.33	0.25	0.14		0.048	0.05
	0.13523 - 0.3	**2**		1	0.33	0.20	0.14			0.07

	0.3 - 0.6	**3**			1	0.33	0.20				0.13
	0.6 - 1.2	**4**				1	0.33				0.25
	>1.2	**5**					1				0.51
TWI	<5	**1**	1	3	5	6	7			0.050	0.49
	05-07.0	**2**		1	3	5	7				0.27
	07-09.0	**3**			1	2	5				0.13
	09-11.0	**4**				1	2				0.07
	>11	**5**					1				0.04
Rainfall (mm/year)	<2200	**1**	1	0.50	0.33	0.20	0.14			0.044	0.05
	2200 - 3500	**2**		1	0.33	0.20	0.14				0.07
	3500 - 4800	**3**			1	0.33	0.20				0.13
	4800 - 6100	**4**				1	0.33				0.26
	>6100	**5**					1				0.50
Soil texture	Loam	**1**	1	0.50	0.17	0.14				0.037	0.06
	Sandy clay	**2**		1	0.17	0.14					0.08
	Clay loam	**3**			1	0.50					0.34
	Clay	**4**				1					0.52
Geomorphology	MDHV	**1**	1	5	4	7	7	3	1	0.052	0.29
	HDP	**2**		1	0.33	3	3	0.33	0.14		0.06
	MDP	**3**			1	3	3	0.33	0.14		0.09
	PC	**4**				1	1	0.20	0.14		0.03
	AP	**5**					1	0.20	0.14		0.03
	W	**6**						1	0.25		0.15
	HDHV	**7**							1		0.35
Lithology	Cn	**1**	1	0.50	0.20	0.14	0.33	0.33		0.030	0.04
	Neo	**2**		1	0.25	0.20	0.50	0.33			0.06
	Pl	**3**			1	0.33	3	2			0.22
	Ms	**4**				1	5	5			0.45
	LcP	**5**					1	1			0.10
	Pr	**6**						1			0.12

352

353 **Table 7** Pairwise comparison matrix and the weight assigned to each landslide conditioning factor by AHP

S. No.	Conditioning Factors	1	2	3	4	5	6	7	8	9	10	11	12	13	14	15	Criteria Weight ($W_{j,AHP}$)
1	Slope	1	4	2	3	5		6	3	4	2	3	4	3	3	2	0.156
2	Aspect		1	3	2	2	0.33	2	0.33	1	0.33	0.50	1	0.50	0.33	0.33	0.046
3	Elevation			1	2	3	2	6	2	3	1	2	2	1	0.50	0.33	0.078
4	Plan curvature				1	2	0.50	2	1	2	0.33	0.50	1	0.50	0.50	0.50	0.040
5	Distance from river					1	0.20	1	0.50	1	0.50	0.25	1	0.50	0.33	0.20	0.025
6	Distance from road						1	3	2	3	2	3	2	1	2.00	0.50	0.094
7	Distance from faults							1	0.50	1	0.25	0.20	1	0.33	0.25	0.14	0.021
8	TWI								1	2	0.50	1	2	0.50	0.33	0.33	0.048
9	SPI									1	0.33	0.33	0.50	0.33	0.33	0.25	0.025
10	LULC										1	2	2	2	0.50	0.50	0.080
11	NDVI											1	3	2	1	0.50	0.070
12	Soil texture												1	0.50	0.33	0.20	0.032
13	Geomorphology													1	0.50	0.33	0.061
14	Lithology														1	0.50	0.090
15	Rainfall															1	0.135
	CR																**0.049**

354

3.2.4. Fuzzy-AHP (FAHP)

In this method, a fuzzy pairwise comparison matrix is constructed based on the linguistic variables defined by the triangular fuzzy scale number (TFN) in Table 3 (Kannan et al. 2013). Five fundamental methods of Fuzzy-AHP are frequently employed in various decision-making studies (Pehlivan et al. 2017). FAHP, using a geometric mean method developed by Buckley (1985), is employed in the present study. It is an extension of AHP using the linguistic variables, and the steps involved are summarised below (Buckley 1985; Pehlivan et al. 2017):

Step 1: Fuzzification

Fuzzification is the conversion of a linguistic term into a membership function. A triangular membership function is shown in Fig. 4. The parameter l_1, m_1, u_1 denotes the lowest value, most likely value (middle value), and the upper value that forms a fuzzy value (μ_A, e.g., $\mu_{A,11} = (l_1, m_1, u_1)$) and is called TFN (Kahraman et al. 2003).

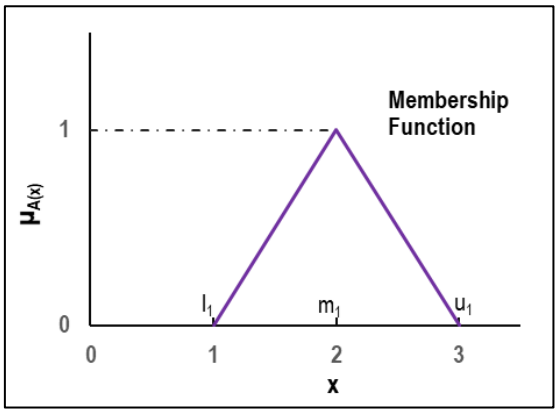

Fig. 4. Triangular membership function (TFN)

Using TFN, a pairwise comparison matric $\tilde{M} = [\mu_{ij}]$ is constructed (Table 8 & 9).

371 $$\tilde{M} = \begin{bmatrix} (1,1,1) & \mu_{12} & \cdots & \mu_{1n} \\ \mu_{21} & (1,1,1) & \cdots & \mu_{2n} \\ \vdots & \cdots & \ddots & \vdots \\ \mu_{n1} & \mu_{n2} & \cdots & (1,1,1) \end{bmatrix}_{n \times n} \quad (14)$$

372 Where $\mu_{ij} = (l_{ij}, m_{ij}, u_{ij})$, $i, j = 1, 2, ..., n$ is TFN.

373 Step 2: Calculation of fuzzy geometric mean value (r_i) for i^{th} criteria

374 $$\tilde{r}_i = (\mu_{i1} \times \mu_{i2} \times \cdots \times \mu_{in})^{(1/n)} \quad (15)$$

375 Step 3: For each criterion, calculation of fuzzy weights (w_i)

376 $$\tilde{w}_i = \tilde{r}_i \times \left(\sum \tilde{r}_i\right)^{(-1)} \quad (16)$$

377 Where $\left(\sum \tilde{r}_i\right)^{(-1)} = \left(\frac{1}{\sum u_i}, \frac{1}{\sum m_i}, \frac{1}{\sum l_i}\right)$

378 Step 4: De-Fuzzification

379 In this step, the fuzzy weights are de-fuzzified using the center of area (COA) method

380 $$w_i = \left(\frac{l_i + m_i + u_i}{3}\right) \quad (17)$$

381 Where w_i is non-fuzzy weights.

382 The normalized de-fuzzified weights are obtained for both conditioning factors ($W_{j,FAHP}$) and
383 their classes ($w_{ij,FAHP}$). These weights are integrated using Equation 18 and used to generate
384 LSM (Fig. 9). In the past, very few landslide susceptibility studies have been performed using
385 the FAHP model (Roodposhti et al. 2014; Mallick et al. 2018; Sur et al. 2020).

386 $$LSM_{FAHP} = \sum_{j=1}^{n} \sum_{i=1}^{m} (w_{ij,FAHP} \times W_{j,FAHP}) \quad (18)$$

387 The landslide susceptibility maps obtained using all the methods are classified into five
388 susceptibility classes (very low, low, moderate, high, and very high) based on the natural breaks
389 classification system (Pourghasemi et al. 2012b) (Fig. 5, 6, 7 & 8).

390 **3.3. Validation of models**

391 In susceptibility studies, model validation is a non-disposable step that suggests the prediction
392 accuracy of the model. For validating the models, produced LSM are compared with testing
393 landslide dataset (30% of landslide inventory) locations. The receiver operating characteristics
394 (ROC) curve is plotted, which represents the true positives (sensitivity) versus false positives
395 (specificity), and AUC (area under the curve) is utilized for prediction accuracy assessment
396 (Ayalew and Yamagishi 2005; Mathew et al. 2009). Higher AUC values imply a better model,
397 and its value range from 0.5 to 1 (Shahabi and Hashim 2015). If AUC is more than 0.8, it is
398 considered a good fit (Yilmaz 2009). Fig. 10 shows the ROC curve for all four models used in
399 the study.

400 **4. Results and discussion**

401 4.1. Identification of most influential factors and their classes

402 In GIS-based susceptibility studies, it is essential to identify the relative influence of each
403 conditioning factor and its classes on the occurrence of the event. The weights corresponding
404 to each factor and their classes are calculated using FR and SE method, listed in Table 5. The
405 FR value shows a spatial correlation between factors and landslide inventory. Therefore, it is
406 assumed that the higher the FR, the larger the influence of a particular factor on the landslide.
407 In the present study, pixels with slopes equal to or greater than 30° have higher FR than others.

In AHP and FAHP models, the subcategory of 30°-40° and >40° slope also show more significant influence than others (Table 6 and 9). In the case of FR and SE model, subfactor of bare land of LULC, clay of soil texture, Mesozoic of factor lithology, and areas with SPI>1.2, TWI<5, rainfall>6100 mm/year in the study region are showing greater susceptibility for landslide than other class categories of the respective conditioning factors (Table 5). Among 15 conditioning factors, slope, LULC, TWI, SPI, lithology are the most influential factors as per the FR model. In the SE model, along with these factors, soil texture also shows a significant influence on landslide occurrence (Table 5). Using AHP, conditioning factors, such as slope, rainfall, distance from road, lithology, and LULC are found with higher weight share than others, while the distance from fault is found with the least weightage (Table 7). In the FAHP model, the dominant landslide factors remain the same as AHP (Table 8).

4.2. Spatial distribution Landslide susceptibility using selected models

The present study employs the four susceptibility models, namely frequency ratio, Shannon entropy, AHP, and fuzzy-AHP, to develop the LSM of Meghalaya. For this purpose, 15 landslide conditioning factors and landslide training datasets are used in the model construction. The result shows that the area under the southern escarpment and southeast portion of the study area has moderate to very high susceptibility for landslide in all four cases (Figs. 5, 6, 8, and 9). According to the FR model (Fig. 5), 2.17%, 5.98%, and 13.10% areas of the total study region are classified as very high, high, and moderate susceptibility categories, respectively (Fig. 7). For the SE model (Fig. 6), 2.07%, 5.38%, and 10.87% areas have very high, high, and moderate susceptibility classes. Similarly, using the AHP model (Fig. 8), 4.01%, 12.04%, and 26.85% area falls under very high, high, and moderate susceptibility classes, respectively. For the FAHP model (Fig. 9), 3.88% and 12.15% area (second largest after AHP) show very high and high susceptibility categories. In comparison, 27.35% area shows moderate susceptibility to landslide, the highest among all four models (Fig. 7). Along

433 with the southern escarpment and southeast region of the study area, these classes are
434 concentrated along highways of the study area in the case of AHP and FAHP models (Fig. 8
435 and 9).

436 4.3. Validation of landslide susceptibility maps

437 The LSM produced using adopted models is validated using the receiver operating
438 characteristics (ROC) curves and the AUC method. For this purpose, 397 landslide testing
439 datasets are used. The ROC curve can also be drawn using a training dataset called the *success*
440 *rate curve*; however, the success rate is not a correct method for evaluating the prediction
441 capability of the models (Pourghasemi et al. 2012b). Therefore, ROC using the testing dataset
442 only is adopted in the present study. The ROC curve produced using the testing dataset
443 (prediction curve) for all four models is shown in Fig. 10. On comparing the AUC values, the
444 AHP model demonstrates the highest prediction accuracy (AUC = 0.913). For FAHP, FR, and
445 SE models, AUC values are 0.903, 0.896, and 0.888, respectively. However, all the models
446 show good prediction accuracy as the AUC value is more than 0.8 in all four cases.

447 4.4. Discussion

448 For landslide hazard assessment and risk mitigation, landslide susceptibility mapping is one of
449 the most applied approaches. The outcome of such susceptibility studies depends upon the
450 applied conditioning factors (Nohani et al. 2019). However, there are no fixed criteria for
451 selecting the conditioning factors at present (Pham et al. 2019b). Therefore, based on the
452 published literature on landslide susceptibility and past landslide characteristics, 15 landslide
453 conditioning factors are adopted in the present study. Among the selected set of factors, slope
454 (degrees) is found as the most significant factor influencing landslides in the area. In this study,
455 the landsides are primarily associated with the locations having slope ranges from 30°-40° and
456 >40°, similar to Mathew et al. 2008. Other than Slope, Lithology, LULC, Rainfall, TWI, and

Distance from Road are also identified as critical factors influencing landslides, consistent with the previous studies (Pourghasemi et al. 2012b; Shahabi and Hashim 2015; Chen and Li 2020).

The present study applies prevalent and widely used bivariate statistical models (FR and SE) and MCDA (AHP and FAHP) for LSM of Meghalaya, India. The prediction power of each model is obtained using a testing dataset. We identified AHP (AUC_{AHP} = 0.913) as the best model following FAHP (0.903), FR (0.896), and SE (0.888) for considered study area. Kavzoglu et al. 2013 also reported the MCDA model (AHP) as a better model than other applied models in their study. Some studies reported fuzzy-AHP as a better model than AHP (Mallick et al. 2018; Sur et al. 2020). Zhao et al. 2017 also compared fuzzy-based SE and AHP models and reported SE with higher prediction accuracy than fuzzy AHP. In Fuzzy-AHP, the fuzzy comparison matrix lacks consistency (Duru et al. 2012), which may explain the better performance of AHP over FAHP in the present study. The prediction accuracy of SE is comparable to that of FR in the present study (Fig. 10), which is consistent with others (Youssef et al. 2015 and Nohani et al. 2019). However, the spatial distribution of high to very high landslide susceptibility class for all four models is approximately consistent and concentrated along the southern-escarpment and southeast portion of the study area.

The findings in the present study can be used for the estimation of the socioeconomic vulnerability to landslides in the study area in terms of socioeconomic losses and downtime (Agrawal et al. 2021). Overall, all four models are acceptable for the landslide susceptibility study of Meghalaya. The landslide susceptibility study is data-driven and controlled by geologic conditions, anthropogenic activity, and LULC. Therefore, the study has some inherent limitations, which can be reduced by applying a high-resolution dataset with advanced data mining techniques and considering temporal variations in the dataset.

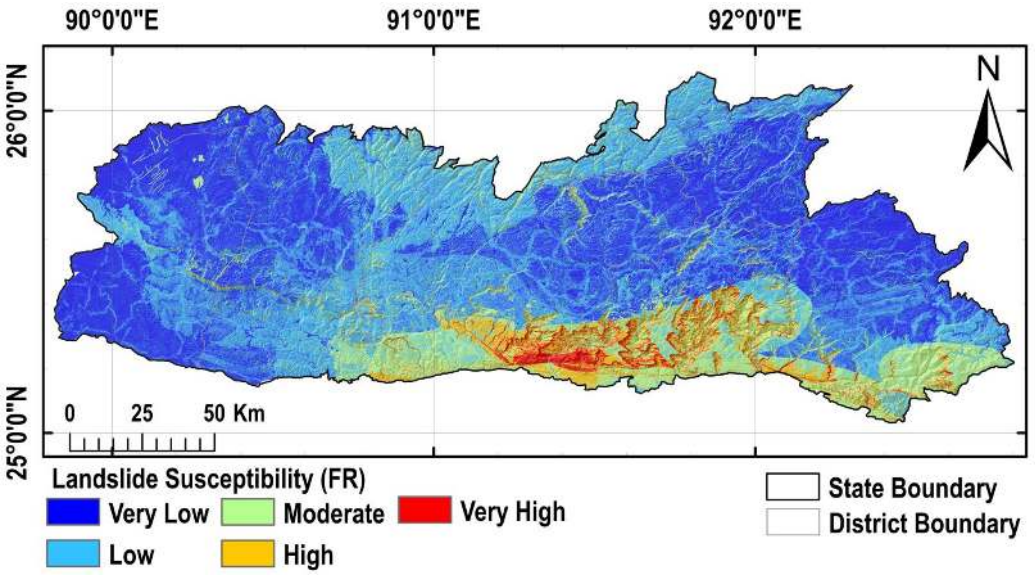

480

481 **Fig. 5** Landslide susceptibility map of Meghalaya using frequency ratio

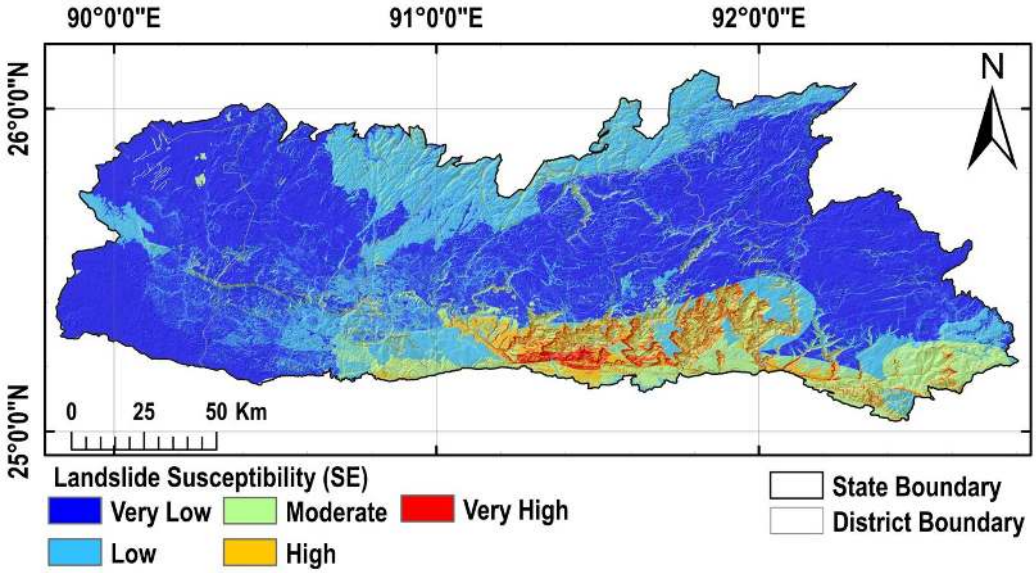

482

483 **Fig. 6** Landslide susceptibility map of Meghalaya using Shannon entropy

484

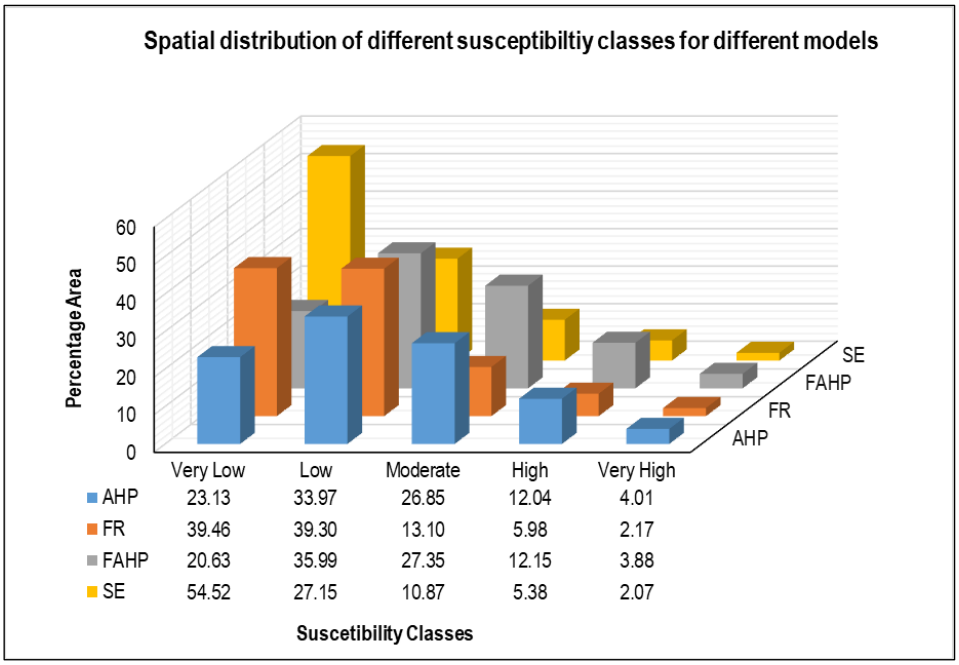

485

486 **Fig. 7** Distribution of different susceptibility classes in the study area

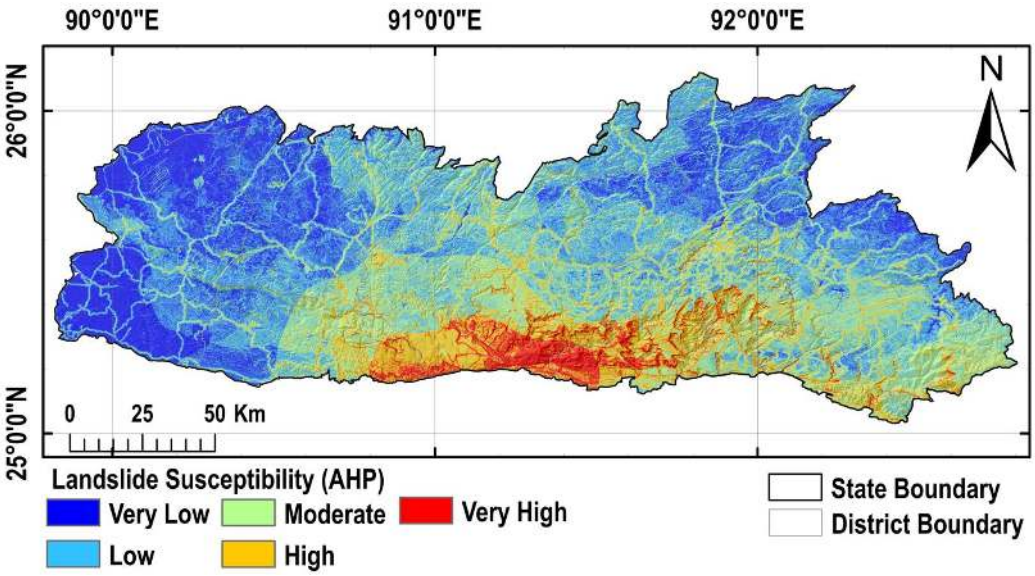

487

488 **Fig. 8** Landslide susceptibility map of Meghalaya using AHP

489

Table 8 Fuzzy-Comparison matrix using TFN, and the weight assigned to each conditioning factor using geometric mean FAHP

Sl. No.	Conditioning Factor	1			2			3			4			5			6			7			8		
1	Slope (degrees)	1	1	1	3	4	5	1	2	3	2	3	4	4	5	6	1	2	3	5	6	7	2	3	4
2	Aspect				1	1	1	2	3	4	1	2	3	1	2	3	0.25	0.33	0.5	1	2	3	0.25	0.33	0.5
3	Elevation							1	1	1	1	2	3	2	3	4	1	2	3	5	6	7	1	2	3
4	Plan curvature										1	1	1	1	2	3	0.33	0.5	1	1	2	3	1	1	1
5	Distance from river													1	1	1	0.17	0.2	0.25	1	1	1	0.33	0.5	1
6	Distance from road																1	1	1	2	3	4	1	2	3
7	Distance from faults																			1	1	1	0.33	0.5	1
8	TWI																						1	1	1
9	SPI																								
10	LULC																								
11	NDVI																								
12	Soil texture																								
13	Geomorphology																								
14	Lithology																								
15	Rainfall (mm/year)																								

Table 8 (continued)

496

497

Sl. No.	Conditioning Factor	9			10			11			12			13			14			15			$W_{j,FAHP}$
1	Slope (degrees)	3	4	5	1	2	3	2	3	4	3	4	5	2	3	4	2	3	4	1	2	3	0.154
2	Aspect	1	1	1	0.25	0.33	0.50	0.33	0.50	1	1	1	1	0.33	0.50	1	0.25	0.33	0.50	0.25	0.33	0.50	0.040
3	Elevation	2	3	4	1	1	1	1	2	3	1	2	3	1	1	1	0.33	0.50	1	0.25	0.33	0.50	0.072
4	Plan curvature	1	2	3	0.25	0.33	0.50	0.33	0.50	1	1	1	1	0.33	0.50	1	0.33	0.50	1	0.33	0.50	1	0.043
5	Distance from river	1	1	1	0.33	0.50	1	0.20	0.25	0.33	1	1	1	0.33	0.50	1	0.25	0.33	0.50	0.17	0.20	0.25	0.026
6	Distance from road	2	3	4	1	2	3	2	3	4	1	2	3	1	1	1	1	2	3	0.33	0.50	1	0.092
7	Distance from faults	1	1	1	0.20	0.25	0.33	0.17	0.20	0.25	1	1	1	0.25	0.33	0.50	0.20	0.25	0.33	0.13	0.14	0.17	0.022
8	TWI	1	2	3	0.33	0.50	1	1	1	1	1	2	3	0.33	0.50	1	0.25	0.33	0.50	0.25	0.33	0.50	0.050
9	SPI	1	1	1	0.25	0.33	0.50	0.25	0.33	0.50	0.33	0.50	1	0.25	0.33	0.50	0.25	0.33	0.50	0.20	0.25	0.33	0.027
10	LULC				1	1	1	1	2	3	1	2	3	1	2	3	0.33	0.50	1	0.33	0.50	1	0.082
11	NDVI							1	1	1	2	3	4	1	2	3	1	1	1	0.33	0.50	1	0.069
12	Soil texture										1	1	1	0.33	0.50	1	0.25	0.33	0.50	0.17	0.20	0.25	0.034
13	Geomorphology													1	1	1	0.33	0.50	1	0.25	0.33	0.50	0.062
14	Lithology																1	1	1	0.33	0.50	1	0.090
15	Rainfall (mm/year)																			1	1	1	0.136

498

499 **Table 9** Fuzzy-comparison matrix for different class of each conditioning factors and weight assigned to each class by FAHP

Conditioning Factors	Classes		1			2			3			4			5		
Slope(degree)	<10°	1	1	1	1	0.33	0.50	1	0.25	0.33	0.50	0.17	0.20	0.25	0.13	0.14	0.17

	10° - 20°	**2**				1	1	1	0.33	0.50	1	0.25	0.33	0.50	0.17	0.20	0.25
	20° - 30°	**3**							1	1	1	0.33	0.50	1	0.25	0.33	0.50
	30° - 40°	**4**										1	1	1	0.25	0.33	0.50
	>40°	**5**													1	1	1
Aspect	Flat (-1)	**1**	1	1	1	0.11	0.11	0.11	0.11	0.11	0.11	0.11	0.13	0.14	0.11	0.13	0.14
	North (0-22.5)	**2**				1	1	1	1	1	1	1	2	3	2	3	4
	Northeast (22.5-67.5)	**3**							1	1	1	1	2	3	1	2	3
	East (67.5-112.5)	**4**										1	1	1	1	1	1
	Southeast (112.5-157.5)	**5**													1	1	1
	South (157.5-202.5)	**6**															
	Southwest (202.5-247.5)	**7**															
	West (247.5-292.5)	**8**															
	Northwest (292.5-337.5)	**9**															
Elevation	<300	**1**	1	1	1	1	1	1	0.33	0.50	1	0.33	0.50	1	0.17	0.20	0.25
	300 - 500	**2**				1	1	1	0.25	0.33	0.50	0.33	0.50	1	0.25	0.33	0.50
	500 - 700	**3**							1	1	1	1	1	1	0.20	0.25	0.33
	700 - 900	**4**										1	1	1	0.33	0.50	1
	900 - 1100	**5**													1	1	1
	1100 - 1300	**6**															
	1300 - 1500	**7**															
	>1500	**8**															
Plan curvature	Concave (<-0.05)	**1**	1	1	1	3	4	5	1	1	1						
	Flat (-0.05-0.05)	**2**				1	1	1	0.20	0.25	0.33						
	Convex (>0.05)	**3**							1	1	1						
Distance from river (m)	<150	**1**	1	1	1	0.33	0.50	1	1	2	3	1	2	3	2	3	4
	150 - 300	**2**				1	1	1	1	2	3	2	3	4	3	4	5
	300 - 450	**3**							1	1	1	1	2	3	2	3	4
	450 - 600	**4**										1	1	1	1	2	3
	>600	**5**													1	1	1

Distance from road (m)	<150	**1**	1	1	1	1	2	3	2	3	4	3	4	5	4	5	6
	150 - 300	**2**				1	1	1	1	2	3	2	3	4	3	4	5
	300 - 450	**3**							1	1	1	1	2	3	2	3	4
	450 - 600	**4**										1	1	1	1	2	3
	>600	**5**													1	1	1
Distance from faults (m)	<1000	**1**	1	1	1	1	1	1	1	2	3	1	2	3	2	3	4
	1000 - 2000	**2**				1	1	1	1	1	1	2	3	4	3	4	5
	2000 - 3000	**3**							1	1	1	1	2	3	2	3	4
	3000 - 4000	**4**										1	1	1	1	2	3
	>4000	**5**													1	1	1
LULC	Waterbodies	**1**	1	1	1	0.33	0.50	1	0.20	0.25	0.33	0.33	0.50	1	0.17	0.20	0.25
	Dense Vegetation	**2**				1	1	1	0.25	0.33	0.50	0.25	0.33	0.50	0.25	0.33	0.50
	Light Vegetation	**3**							1	1	1	1	2	3	1	2	3
	Agricultural Land	**4**										1	1	1	0.25	0.33	0.50
	Built Area	**5**													1	1	1
	Bare Land	**6**															
NDVI	<0.015	**1**	1	1	1	0.14	0.17	0.20	0.14	0.17	0.20	0.25	0.33	0.50	0.25	0.33	0.50
	0.015 - 0.14	**2**				1	1	1	0.33	0.50	1	1	2	3	2	3	4
	0.14 - 0.18	**3**							1	1	1	1	2	3	2	3	4
	0.18 - 0.27	**4**										1	1	1	1	2	3
	0.27 - 0.36	**5**													1	1	1
	0.36 - 0.999	**6**															
SPI	< 0.13523	**1**	1	1	1	0.33	0.50	1	0.25	0.33	0.50	0.20	0.25	0.33	0.13	0.14	0.17
	0.13523 - 0.3	**2**				1	1	1	0.25	0.33	0.50	0.17	0.20	0.25	0.13	0.14	0.17
	0.3 - 0.6	**3**							1	1	1	0.25	0.33	0.50	0.17	0.20	0.25
	0.6 - 1.2	**4**										1	1	1	0.25	0.33	0.50
	>1.2	**5**													1	1	1
TWI	<5	**1**	1	1	1	2	3	4	4	5	6	5	6	7	6	7	8
	05-07.0	**2**				1	1	1	2	3	4	4	5	6	6	7	8

	07-09.0	**3**						1	1	1	1	2	3	4	5	6
	09-11.0	**4**									1	1	1	1	2	3
	>11	**5**												1	1	1
Rainfall	<2200	**1**	1	1	1	0.33	0.50	1	0.25	0.33	0.50	0.17	0.20	0.25	0.13	0.14	0.17
	2200 - 3500	**2**				1	1	1	0.25	0.33	0.50	0.17	0.20	0.25	0.13	0.14	0.17
	3500 - 4800	**3**							1	1	1	0.25	0.33	0.50	0.17	0.20	0.25
	4800 - 6100	**4**										1	1	1	0.25	0.33	0.50
	>6100	**5**													1	1	1
Soil texture	Loam	**1**	1	1	1	0.33	0.50	1	0.14	0.17	0.20	0.13	0.14	0.17			
	Sandy Clay	**2**				1	1	1	0.14	0.17	0.20	0.13	0.14	0.17			
	Clay Loam	**3**							1	1	1	0.33	0.50	1			
	Clay	**4**										1	1	1			
Geomorphology	MDHV	**1**	1	1	1	4	5	6	3.00	4.00	5.00	6	7	8	6	7	8
	HDP	**2**				1	1	1	0.25	0.33	0.50	2	3	4	2	3	4
	MDP	**3**							1	1	1	2	3	4	2	3	4
	PC	**4**										1	1	1	1	1	1
	AP	**5**													1	1	1
	W	**6**															
	HDHV	**7**															
Lithology	Cn	**1**	1	1	1	0.33	0.50	1	0.17	0.20	0.25	0.13	0.14	0.13	0.25	0.33	0.50
	Neo	**2**				1	1	1	0.20	0.25	0.33	0.17	0.20	0.25	0.33	0.50	1
	Pl	**3**							1	1	1	0.25	0.33	0.50	2	3	4
	Ms	**4**										1	1	1	4	5	6
	LcP	**5**													1	1	1
	Pr	**6**															

Table 9 (continued)

Conditioning Factors	**Classes**	**6**	**7**	**8**	**9**	**$w_{ij,FAHP}$**

Slope(degree)	<10°	**1**												0.054
	10° - 20°	**2**												0.091
	20° - 30°	**3**												0.157
	30° - 40°	**4**												0.237
	>40°	**5**												0.461
Aspect	Flat (-1)	**1**	0.11	0.13	0.14	0.11	0.13	0.14	0.125	0.143	0.167	0.13	0.14	0.17	0.013
	North (0-22.5)	**2**	2	3	4	3	4	5	4	5	6	3	4	5	0.228
	Northeast (22.5-67.5)	**3**	2	3	4	1	2	3	2	3	4	2	3	4	0.186
	East (67.5-112.5)	**4**	1	2	3	1	2	3	5	6	7	6	7	8	0.160
	Southeast (112.5-157.5)	**5**	1	1	1	1	2	3	4	5	6	2	3	4	0.131
	South (157.5-202.5)	**6**	1	1	1	1	1	1	2	3	4	2	3	4	0.103
	Southwest (202.5-247.5)	**7**				1	1	1	2	3	4	1	2	3	0.091
	West (247.5-292.5)	**8**							1	1	1	0.33	0.50	1	0.039
	Northwest (292.5-337.5)	**9**										1	1	1	0.051
Elevation	<300	**1**	0.17	0.20	0.25	0.17	0.20	0.25	0.25	0.33	0.50				0.043
	300 - 500	**2**	0.20	0.25	0.33	0.20	0.25	0.33	0.25	0.33	0.50				0.046
	500 - 700	**3**	0.20	0.25	0.33	0.17	0.20	0.25	0.33	0.50	1				0.068
	700 - 900	**4**	0.25	0.33	0.50	0.25	0.33	0.50	0.25	0.33	0.50				0.076
	900 - 1100	**5**	1	1	1	0.33	0.50	1	0.33	0.50	1				0.160
	1100 - 1300	**6**	1	1	1	1	1	1	1	2	3				0.212
	1300 - 1500	**7**				1	1	1	1	2	3				0.234
	>1500	**8**							1	1	1				0.161
Plan curvature	Concave (<-0.05)	**1**													0.443
	Flat (-0.05-0.05)	**2**													0.115
	Convex (>0.05)	**3**													0.443
Distance from river (m)	<150	**1**													0.247

	150 - 300	**2**						0.355
	300 - 450	**3**						0.195
	450 - 600	**4**						0.128
	>600	**5**						0.075
Distance from road (m)	<150	**1**						0.402
	150 - 300	**2**						0.267
	300 - 450	**3**						0.166
	450 - 600	**4**						0.101
	>600	**5**						0.064
Distance from faults (m)	<1000	**1**						0.283
	1000 - 2000	**2**						0.279
	2000 - 3000	**3**						0.223
	3000 - 4000	**4**						0.135
	>4000	**5**						0.080
LULC	Waterbodies	**1**	0.14	0.17	0.20			0.048
	Dense Vegetation	**2**	0.17	0.20	0.25			0.065
	Light Vegetation	**3**	0.25	0.33	0.50			0.202
	Agricultural Land	**4**	0.20	0.25	0.33			0.105
	Built Area	**5**	0.25	0.33	0.50			0.183
	Bare Land	**6**	1	1	1			0.397
NDVI	<0.015	**1**	0.33	0.50	1.00			0.046
	0.015 - 0.14	**2**	3	4	5			0.267
	0.14 - 0.18	**3**	3	4	5			0.325
	0.18 - 0.27	**4**	2	3	4			0.177
	0.27 - 0.36	**5**	2	3	4			0.121
	0.36 - 0.999	**6**	1	1	1			0.065
SPI	< 0.13523	**1**						0.052
	0.13523 - 0.3	**2**						0.063
	0.3 - 0.6	**3**						0.126

	0.6 - 1.2	**4**							0.252
	>1.2	**5**							0.507
TWI	<5	**1**							0.485
	05-07.0	**2**							0.277
	07-09.0	**3**							0.126
	09-11.0	**4**							0.071
	>11	**5**							0.041
Rainfall	<2200	**1**							0.049
	2200 - 3500	**2**							0.062
	3500 - 4800	**3**							0.125
	4800 - 6100	**4**							0.261
	>6100	**5**							0.502
Soil texture	Loam	**1**							0.057
	Sandy Clay	**2**							0.077
	Clay Loam	**3**							0.353
	Clay	**4**							0.513
Geomorphology	MDHV	**1**	2	3	4	1	1	1	0.297
	HDP	**2**	0.25	0.33	0.50	0.13	0.14	0.17	0.059
	MDP	**3**	0.25	0.33	0.50	0.13	0.14	0.13	0.081
	PC	**4**	0.17	0.20	0.25	0.13	0.14	0.13	0.032
	AP	**5**	0.17	0.20	0.25	0.13	0.14	0.13	0.032
	W	**6**	1	1	1	0.20	0.25	0.33	0.148
	HDHV	**7**				1	1	1	0.351
Lithology	Cn	**1**	0.25	0.33	0.50				0.043
	Neo	**2**	0.25	0.33	0.50				0.065
	Pl	**3**	1	2	3				0.225
	Ms	**4**	4	5	6				0.442
	LcP	**5**	1	1	1				0.104
	Pr	**6**	1	1	1				0.121

502

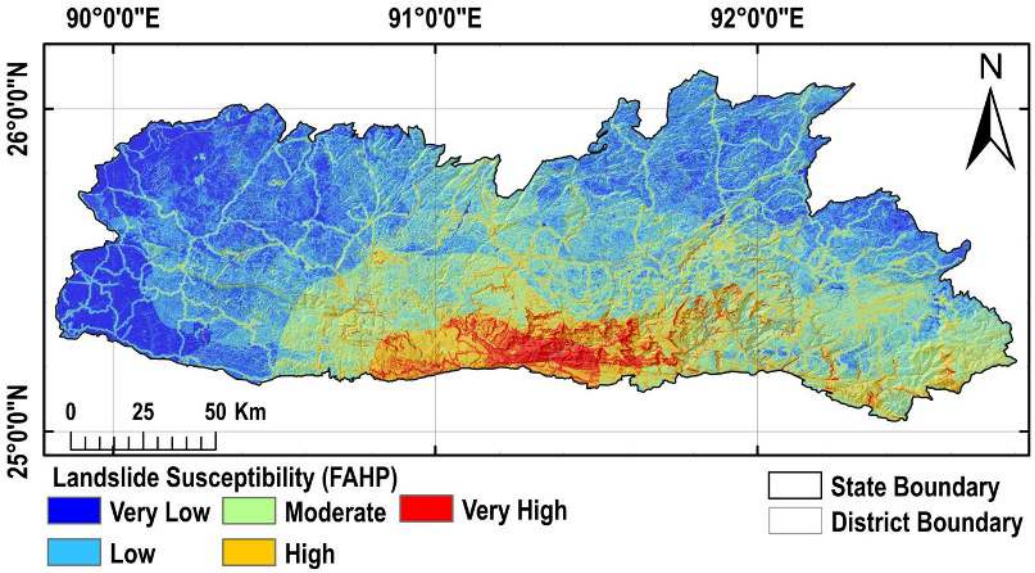

Fig. 9 Landslide susceptibility map of Meghalaya using FAHP

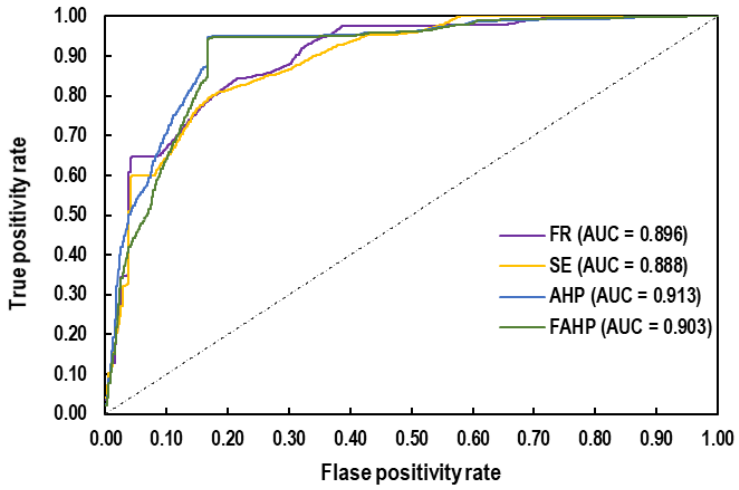

Fig. 10 ROC curve for all four models using the testing dataset

5. Conclusion

In this study, FR, SE, AHP, and FAHP models are used to generate the landslide susceptibility map of Meghalaya state in NER of India. The landslide inventory consisting of 1330 landslide data points is prepared and distributed into a 70/30 ratio to form training and testing datasets. Based on the present study, slope is found as the most influencing factor among the selected

15 conditioning factors. The performance of each model is evaluated by the AUC value based on the testing dataset. The results showed that the prediction accuracy of the AHP model is better than the other three models in the present study, with an AUC value of 0.913 (91.3% prediction accuracy). The produced LSMs reveals that the southern escarpment of the study area, the area in the southeast, and hillslopes along the roads possess great susceptibility for future landslides. If the road network gets affected due to landslide events, the intra-district/state, inter-district/state connectivity get hampered and impart substantial economic losses to the population in the region. Therefore, the presented LSM for the considered study area can help the authorities and decision-makers to plan and manage the risk mitigation strategies for future landslides and plan the sustainable infrastructure development in the region accordingly.

Declaration of Competing Interests

The authors declare that they have no known competing financial interests or non-financial interests or personal relationships that are directly or indirectly related to the work submitted for publication that could have appeared to influence the work reported in this paper.

References

1. Agrawal N, Gupta L, Dixit J (2021) Assessment of the Socioeconomic Vulnerability to Seismic Hazards in the National Capital Region of India Using Factor Analysis. Sustainability 13(17):9652
2. Akgun A, Sezer EA, Nefeslioglu HA, Gokceoglu C, Pradhan B (2012) An easy-to-use MATLAB program (MamLand) for the assessment of landslide susceptibility using a Mamdani fuzzy algorithm. Computers & Geosciences 38(1):23-34

535 3. Ayalew L, Yamagishi H (2005) The application of GIS-based logistic regression for
536 landslide susceptibility mapping in the Kakuda-Yahiko Mountains, Central Japan.
537 Geomorphology 65(1-2):15–31
538 4. Bhukosh-Geological Survey India (2021) URL https://bhukosh.gsi.gov.in/
539 Bhukosh/MapViewer.aspx (Last accessed: 10 September 2021)
540 5. Bordoni M, Galanti Y, Bartelletti C, Persichillo MG, Barsanti M, Giannecchini R,
541 Avanzi GDA, Cevasco A, Brandolini P, Galve JP, Meisina C (2020) The influence of
542 the inventory on the determination of the rainfall-induced shallow landslides
543 susceptibility using generalized additive models. Catena 193:104630
544 6. Buckley JJ (1985) Fuzzy hierarchical analysis. Fuzzy sets and systems 17(3):233-247
545 7. Can T, Nefeslioglu HA, Gokceoglu C, Sonmez H, Duman TY (2005) Susceptibility
546 assessments of shallow earthflows triggered by heavy rainfall at three catchments by
547 logistic regression analyses. Geomorphology 72(1-4):250–271
548 8. Chen W, Li Y (2020) GIS-based evaluation of landslide susceptibility using hybrid
549 computational intelligence models. Catena 195:104777
550 9. Chimidi G, Raghuvanshi TK, Suryabhagavan KV (2017) Landslide hazard evaluation
551 and zonation in and around Gimbi town, western Ethiopia-a GIS-based statistical
552 approach. Applied Geomatics 9(4):219–236
553 10. Duru O, Bulut E, Yoshida S (2012) Regime switching fuzzy AHP model for choice-
554 varying priorities problem and expert consistency prioritization: A cubic fuzzy-priority
555 matrix design. Expert Systems with Applications 39(5):4954–4964
556 11. El-Jazouli A, Barakat A, Khellouk R (2019) GIS-multicriteria evaluation using AHP
557 for landslide susceptibility mapping in Oum Er Rbia high basin (Morocco).
558 Geoenvironmental Disasters 6(1):1–12

559 12. Ercanoglu M, Gokceoglu C (2004) Use of fuzzy relations to produce landslide
560 susceptibility map of a landslide prone area. Engineering Geology 75(3- 4):229–250
561 13. Galli M, Ardizzone F, Cardinali M, Guzzetti F, Reichenbach P (2008) Comparing
562 landslide inventory maps. Geomorphology 94:268–289
563 14. Guha-Sapir D, Vos F, Below R, Ponserre S (2012) Annual disaster statistical review
564 2011: the numbers and trends. CRED, Brussels
565 15. Kahraman C, Cebeci U, Ulukan Z (2003) Multi-criteria supplier selection using fuzzy
566 AHP. Logistics Information Management 16(6):382–394
567 16. Kamp U, Growley BJ, Khattak GA, Owen LA (2008) GIS-based landslide
568 susceptibility mapping for the 2005 Kashmir earthquake region. Geomorphology
569 101(4):631–642
570 17. Kannan D, Khodaverdi R, Olfat L, Jafarian A, Diabat A (2013) Integrated fuzzy multi
571 criteria decision making method and multi-objective program- ming approach for
572 supplier selection and order allocation in a green supply chain. Journal of Cleaner
573 Production 47:355–367
574 18. Kanungo DP, Arora MK, Sarkar S, Gupta RP (2006) A comparative study of
575 conventional, ANN black box, fuzzy and combined neural and fuzzy weighting
576 procedures for landslide susceptibility zonation in Darjeeling Himalayas. Engineering
577 Geology 85(3-4):347–366
578 19. Kavzoglu T, Sahin EK, Colkesen I (2014) Landslide susceptibility mapping using GIS-
579 based multi-criteria decision analysis, support vector machines, and logistic regression.
580 Landslides 11(3):425–439
581 20. Kayastha P, Dhital MR, De Smedt F (2013) Application of the analytical hierarchy
582 process (AHP) for landslide susceptibility mapping: A case study from the Tinau
583 watershed, west Nepal. Computers & Geosciences 52:398-408

584 21. Lotfi FH, Fallahnejad R (2010) Imprecise Shannon's entropy and multi attribute
585 decision making. Entropy 12(1):53–62
586 22. Mallick J, Singh RK, Alawadh MA, Islam S, Khan RA, Qureshi MN (2018) GIS-based
587 landslide susceptibility evaluation using fuzzy-AHP multi-criteria decision-making
588 techniques in the Abha Watershed, Saudi Arabia. Environmental Earth Sciences
589 77(7):1–25
590 23. Mathew J, Jha VK, Rawat GS (2009) Landslide susceptibility zonation mapping and
591 its validation in part of Garhwal Lesser Himalaya, India, using binary logistic
592 regression analysis and receiver operating characteristic curve method. Landslides
593 6(1):17–26
594 24. Mattivi P, Franci F, Lambertini A, Bitelli G (2019) TWI computation: a comparison of
595 different open-source GISs. Open Geospatial Data, Software and Standards 4(1):1–12
596 25. Moore ID, Grayson RB, Ladson AR (1991) Digital terrain modelling: a review of
597 hydrological, geomorphological, and biological applications. Hydrological Processes
598 5(1):3–30
599 26. Nohani E, Moharrami M, Sharafi S, Khosravi K, Pradhan B, Pham BT, Lee S, Melesse
600 A (2019) Landslide susceptibility mapping using different GIS-based bivariate
601 models. Water 11(7):1402
602 27. Oh HJ, Pradhan B (2011) Application of a neuro-fuzzy model to landslide-
603 susceptibility mapping for shallow landslides in a tropical hilly area. Computers &
604 Geosciences 37(9):1264–1276
605 28. Onagh M, Kumra VK, Rai PK (2012) Landslide susceptibility mapping in a part of
606 Uttarkashi district (India) by multiple linear regression method. International Journal
607 of Geology, Earth and Environmental Sciences 2(2):102–120

29. Pai DS, Sridhar L, Rajeevan M, Sreejith OP, Satbhai NS, Mukhopadhyay B (2014) Development of a new high spatial resolution (0.25° X 0.25°) long period (1901-2010) daily gridded rainfall data set over India and its comparison with existing data sets over the region. Mausam 65(1):1-18
30. Pareek N, Sharma ML, Arora MK (2010) Impact of seismic factors on landslide susceptibility zonation: a case study in part of Indian Himalayas. Landslides 7(2):191–201
31. Pehlivan NY, Paksoy T, Çalik A (2017) Comparison of methods in FAHP with application in supplier Selection. In Fuzzy Analytic Hierarchy Process, Chapman and Hall/CRC 45-76
32. Pham BT, Prakash I, Khosravi K, Chapi K, Trinh PT, Ngo TQ, Hosseini SV, Bui DT (2019a) A comparison of Support Vector Machines and Bayesian algorithms for landslide susceptibility modelling. Geocarto International 34(13):1385–1407
33. Pham BT, Prakash I, Singh SK, Shirzadi A, Shahabi H, Bui DT (2019b) Landslide susceptibility modeling using Reduced Error Pruning Trees and different ensemble techniques: Hybrid machine learning approaches. Catena 175:203–218
34. Pourghasemi HR, Mohammady M, Pradhan B (2012a) Landslide susceptibility mapping using index of entropy and conditional probability models in GIS: Safarood Basin, Iran. Catena 97:71–84
35. Pourghasemi HR, Pradhan B, Gokceoglu C (2012b) Application of fuzzy logic and analytical hierarchy process (AHP) to landslide susceptibility mapping at Haraz watershed, Iran. Natural Hazards 63(2):965–996
36. Pourghasemi HR, Pradhan B, Gokceoglu C (2012c) Remote sensing data derived parameters and its use in landslide susceptibility assessment using Shannon's entropy and GIS. In Applied Mechanics and Materials 225:486– 491

633 37. Pradhan B, Lee S (2010) Delineation of landslide hazard areas on Penang Island,
634 Malaysia, by using frequency ratio, logistic regression, and artificial neural network
635 models. Environmental Earth Sciences 60(5):1037–1054
636 38. Prokop P (2014) The Meghalaya Plateau: landscapes in the abode of the clouds.
637 Landscapes and landforms of India, Springer pp 173–180
638 39. Reichenbach P, Rossi M, Malamud BD, Mihir M, Guzzetti F (2018) A review of
639 statistically-based landslide susceptibility models. Earth Science Reviews 180:60–91
640 40. Roodposhti MS, Rahimi S, Beglou MJ (2014) PROMETHEE II and fuzzy AHP: an
641 enhanced GIS-based landslide susceptibility mapping. Natural Hazards 73(1):77–95
642 41. Roodposhti MS, Aryal J, Shahabi H, Safarrad T (2016) Fuzzy shannon entropy: A
643 hybrid GIS-based landslide susceptibility mapping method. Entropy 18(10):343
644 42. Saaty TL (2000) Fundamentals of decision making and priority theory with the analytic
645 hierarchy process. In Analytic Hierarchy Process Series 6, RWS Publications,
646 Pittsburgh
647 43. Saaty TL (2008) Decision making with the analytic hierarchy process. International
648 Journal of Services Sciences 1(1):83–98
649 44. Sarkar S, Kanungo DP (2004) An integrated approach for landslide susceptibility
650 mapping using remote sensing and GIS. Photogrammetric Engineering & Remote
651 Sensing, 70(5):617–625
652 45. Shahabi H, Hashim M (2015) Landslide susceptibility mapping using GIS-based
653 statistical models and Remote sensing data in tropical environment. Scientific Reports
654 5(1):1–15
655 46. Shahabi H, Khezri S, Ahmad BB, Hashim M (2014) Landslide susceptibility mapping
656 at central Zab basin, Iran: A comparison between analytical hierarchy process,
657 frequency ratio and logistic regression models. Catena 115:55–70

47. Shano L, Raghuvanshi TK, Meten M (2020) Landslide susceptibility evaluation and hazard zonation techniques-a review. Geoenvironmental Disasters 7:1–19
48. Sur U, Singh P, Meena SR (2020) Landslide susceptibility assessment in a lesser Himalayan road corridor (India) applying fuzzy AHP technique and earth-observation data. Geomatics, Natural Hazards and Risk 11(1):2176–2209
49. USGS (2021) Earth Explorer, https://earthexplorer.usgs.gov/ (last accessed: 10 September 2021)
50. Wang F, Cao Y, Liu M (2011) Risk early-warning method for natural disasters based on integration of entropy and DEA model. Applied Mathematics 2(1): 23
51. Wang LJ, Guo M, Sawada K, Lin J, Zhang J (2015) Landslide susceptibility mapping in Mizunami City, Japan: A comparison between logistic regression, bivariate statistical analysis and multivariate adaptive regression spline models. Catena 135:271–282
52. Yilmaz I (2009) Landslide susceptibility mapping using frequency ratio, logistic regression, artificial neural networks and their comparison: a case study from Kat landslides (Tokat-Turkey). Computers & Geosciences 35(6):1125–1138
53. Youssef AM, Pradhan B, Jebur MN, El-Harbi HM (2015) Landslide suscepti- bility mapping using ensemble bivariate and multivariate statistical models in Fayfa area, Saudi Arabia. Environmental Earth Sciences 73(7):3745–3761
54. Zhao H, Yao L, Mei G, Liu T, Ning Y (2017) A fuzzy comprehensive evaluation method based on AHP and entropy for a landslide susceptibility map. Entropy 19(8):396